The University of South Bohemia in České Budějovice
Faculty of Science

Nitrate isotopes and cycling in Bohemian Forest Lakes.

Bachelor Thesis

Precious Adu Appiah

Supervisor: Travis Blake Meador, Ph.D.

České Budějovice, 2023

Appiah, P.A., 2023: Nitrate isotopes and cycling in the Bohemian Forest Lakes. Bachelor Thesis in English. – 49pp., Faculty of Science, University of South Bohemia, České Budějovice, Czech Republic.

Annotation
This thesis develops and implements novel techniques for tracking nitrate isotopes to identify the major processes, including nitrification and denitrification, in the Bohemian National Forest's pristine Plešné, Čertovo, and Černé Lakes settings. The study optimizes a method for precise isotopic monitoring by conducting a comparative examination of three independent nitrous oxide conversion protocols. The selected method was applied to analyze the lake samples, providing crucial insights into the relative inputs and complicated nitrogen cycling mechanisms inside these unique forest lake ecosystems.

Declaration
I declare that I am the author of this qualification thesis and that in writing it, I have used the sources and literature displayed in the list of used sources only.

České Budějovice, 14/12/2023

.....

Precious Adu Appiah

Acknowledgement
I express my deepest thanks to Travis Blake Meador, Ph. D., my thesis supervisor, for his unwavering leadership, invaluable insights, and steadfast support during my academic quest. His knowledge, patience, and support were valuable in crafting this thesis.

I am also thankful to my co-supervisor, Mgr. Ljubov Poláková, for her insight, constructive input, and devotion to this research project. Her support and guidance have been influential in establishing the scope and direction of this endeavour.

I am grateful to Travis Blake Meador, Ph. D., and Mgr. Ljubov Poláková for their constant encouragement, insightful advice, and unending support during every stage of my thesis. Their advice has been indispensable in refining my ideas and completing this academic milestone successfully.

I also want to thank the Institute of Soil Biology and Biogeochemistry for creating an environment favourable to study and research.

Abstract

Nitrate contamination of waterbodies is a ubiquitous environmental problem stemming from the overloading of reactive nitrogen into aquatic systems. This surplus results from anthropogenic activities, with fertilizer production being the predominant cause. Excess nitrate in surface waterways can cause eutrophication, which promotes excessive algal and plant growth and substantial environmental harm. Consumption of nitrate-polluted water is also a concern for human health, as it can raise the risk of cancers, reproductive issues, and blood oxygen deprivation in infants. The nitrogen sources and processes occurring in diverse water bodies have been an ongoing topic of investigation and environmental monitoring efforts for decades, which have been advanced with the analysis of nitrate isotopic composition. The current study sought to establish and implement a modern method to track nitrate isotopes and constrain the relative inputs and processes (e.g., nitrification and denitrification) happening in the Bohemian National Forest's pristine Plešné, Čertovo, and Černé Lakes. The methodology involved sampling from lake tributaries and outlets, filtering the samples, converting nitrate to nitrous oxide using titanium (III) chloride, and analysis via isotope ratio mass spectrometry. The primary source of nitrate for all lakes was likely atmospheric deposition and mineralization of organic nitrogen; however, the primary nitrogen cycling processes and/or balance of processes appeared to differ between lakes. While the primary process in the Plesne catchment was likely nitrification, nitrate isotopes in the Čertovo catchment suggest that denitrification was a major process. Černé, on the other hand, may have been more influenced by nitrogen fixation. These findings may be used as a baseline for interpreting human impact on other lake catchments.

Contents

List of used abbreviations and symbols.

Ampl: Amplitude

Avg: Average

℃: degrees Celsius

CF-IRMS: Continuous flow Isotope Ratio Mass Spectrometry

cm: Centimeters

CN: Černé

CO_2: Carbon dioxide

ConFlo: Continuous Flow

CT: Čertovo

DI: deionized

DI-IRMS: Dual Inlet Isotope Ratio Mass Spectrometry

δ: Delta value

Fig.: Figure

g: grams

GF/F: glass microfibre filters

H_2: Hydrogen gas

HCl: Hydrochloric acid

He: Helium

IAEA: International Atomic Energy Agency

IRMS: Isotope Ratio Mass Spectrometry

KNO_3: Potassium nitrate

L: Litre

m: meter

mg: milligram

min; minute

mg L^{-1}: milligram per litre

mL min^{-1}: milliliters per minute

mm: millimetres

mol: mole

N: Nitrogen

$NaNO_3$: Sodium Nitrate

NH_3: Ammonia

NH_4^+: Ammonium

N_2O: Nitrous oxide

nm: nanomolar

nmol: nanomole

NO_2^-: Nitrite

NO_3^-: Nitrate

$[NO_3^-]$: Nitrate Concentration

NO_3^--N: Nitrate Nitrogen

Ø: diameter

O: Oxygen

Org N: Organic nitrogen

pers.com.: personal communication

PL: Plešné

ppb: parts per billion

ppm: parts per million

SD: Standard deviation

Ti(IV) : Titanium(IV)

$TiCl_3$: Titanium (III) Chloride

µM: micro-molar

µm: micrometre

USGS: U.S. Geological Survey

% v/v: volume concentration

Vol.: Volume

VSMOW: Vienna Standard Mean Ocean Water

% w/v: mass concentration

Zn: Zinc

1 Theoretical background

Nitrate (NO_3^-) contamination in surface and groundwaters is a global environmental issue primarily resulting from anthropogenic processes (Xu et al., 2015). As a naturally occurring substance that enters the environment through geological and biological processes and since the mid-20th century, industrial processes, NO_3^- is the most abundant reactive nitrogen (N) species in groundwater (Liu et al., 2006). Although NO_3^- pollution is caused by various sources, including mineral N fertilizers and animal manure in agriculture, domestic or industrial N-bearing sewage, atmospheric deposition, mineralization of soil organic N, and biological N fixation (Nestler et al., 2011; O et al., 2013), the overuse of N-based fertilizers in agriculture is one of the primary sources of NO_3^- pollution.

The Haber-Bosch process is widely considered one of the most innovative industrial chemical processes ever devised to produce ammonia (NH_3) through anthropogenic means. The NH_3 produced is then used to generate inorganic fertilizers. These fertilizers allow farmers to enhance crop yield without using more land due to the soil's decreased productivity over time (Hochman et al., 2022). Natural N sources account for only about half of the world's needs (Smil, 1999). Therefore, Fritz Haber and Carl Bosch used large-scale NH_3 synthesis to bridge the gap between the need for naturally fixed N and the agricultural need to feed the world's rising population (Hochman et al., 2022; Smil, 1999). People's capacity to grow food grew substantially as more NH_3 was available to manufacture inorganic fertilizers. Consequently, the Haber-Bosch process, technological advances, and health care increased the world's population (Smil, 1999). However, this increased use of N-based fertilizers has generated major environmental issues. The Haber-Bosch process accumulates reactive N in the biosphere, thereby tilting the balance of the global N cycle. This process leads to an increase in reactive N and threatens ecosystems.

Runoff from N fertilizers can damage biological habitats by dumping NO_3^- into rivers, ponds, and lakes, therewith extending dead sea zones and altering natural ecosystems (Kremser & Schnug, 2002). When excess NO_3^- infiltrates surface waters, it triggers eutrophication (excessive N overload), which causes excessive algal and plant development and significant damage to the aquatic environment (Xu et al., 2015; Nestler et al., 2011). Galloway et al. (2008) state that the consumption of NO_3^--polluted waters is also of concern as it can cause cancer and reproductive risks. Moreover, consuming NO_3^- contaminated water can cause methemoglobinemia, especially in infants (Xu et al., 2015). The World Health Organization has, therefore, set a maximum

permissible level of 10 mg L^{-1} of NO_3^--N for drinking water, while the European Union (E.C., 1998) has developed a maximum limit of 50 mg L^{-1} of NO_3^--N for human intake (Xu et al., 2015).

Understanding water movement and accompanying contaminants becomes critical because groundwater flow pathways are tightly linked with surface water interactions. Because NO_3^- is exceptionally mobile and generally originates from non-point source pollution, it is spread over a vast region via numerous groundwater flow paths, thus making it difficult to pinpoint the source (Kaushal et al.,2011). Effective management practices to conserve water quality and rehabilitation strategies for previously contaminated areas must trace the flow paths to identify actual N sources and know the mechanisms influencing local NO_3^- concentrations($[NO_3^-]$). A deeper understanding of hydrologic flow paths and solute sources is also necessary to estimate the possible impact of pollutants on water supplies (Kendall et al., 2007). The availability of several potential NO_3^- sources in various places, the presence of overlapping point and non-point sources, as well as the coexistence of many biogeochemical processes that change the amounts of NO_3^- and other chemicals complicate the relationship between the amount of NO_3^- delivered from a specific source and NO_3^- concentrations in groundwater and surface water (Kendall et al., 2007).

To address these challenges, scientists have turned to various methods. Though different concentration-based methods, such as biochemical oxygen demand and organic carbon, have been used to trace mixed contamination effectively, this approach does not easily track contaminant movement and physical processes (Alimi et al., 2003). On the other hand, stable isotope analysis is a powerful tool for identifying sources, inferring processes, and determining the contributions of diverse inputs due to its precision, adaptability, and wide range of applications (Michener & Lajtha,2007).

1.1 Understanding the nitrogen cycle and stable isotope analysis.

The succeeding sub-chapter presents theoretical information on the N cycle, stable NO_3^- isotopes, and their analysis.

1.1.1. Nitrogen Cycle

N is one of the six critical elements required for life. It is the most prevalent element in the atmosphere, accounting for 78%. On Earth, there are two significant reserves of N: atmospheric molecular nitrogen (N_2) and biologically reactive N (Takai, 2019). The N cycle is a collection of

biogeochemical processes that outlines how N moves and transforms throughout ecosystems. The cycle comprises five key processes: fixation, nitrification, assimilation, ammonification, and denitrification. The N cycle continues to be investigated to better understand the origins of NO_3^- and the effect of NO_3^- pollution.

The N cycle.

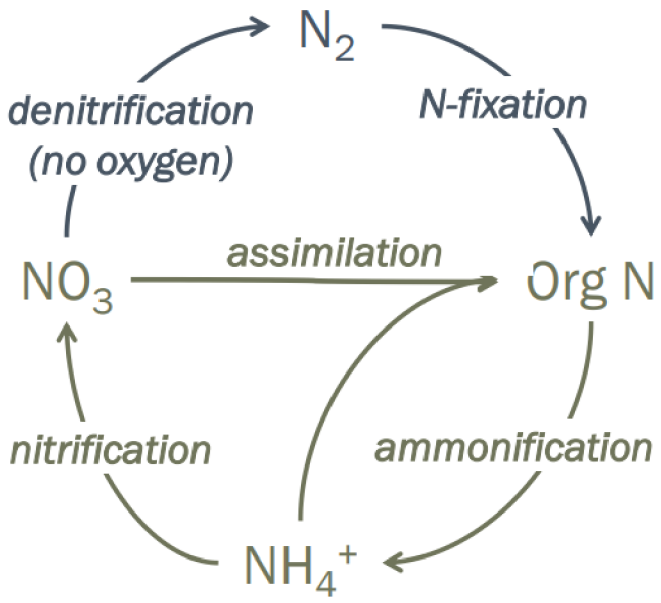

Figure 1: The diagram shows major processes in the N cycle. The blue part (upper part) indicates the "unreactive" N species and processes, while the orange box illustrates the N species and processes involving "reactive" N.

1.1.2. Nitrogen Fixation

Although nitrogen gas is most abundant in the atmosphere, it is in a form that makes its direct usage by most organisms difficult. As a result, atmospheric nitrogen must first be transformed into NH_3 or other N compounds via a process known as N fixation (Takai, 2019) before it can be used for metabolic needs.

Biological N fixation occurs when diazotrophs encode nitrogenase enzyme complexes composed of the molybdenum-iron protein dinitrogenase and the vanadium or iron protein dinitrogenase reductase (Stein & Klotz, 2016). N fixation is particularly oxygen sensitive, hence necessitating the development of protective strategies such as spatial decoupling (compartmentalization or the formation of specialized cells), temporal decoupling, quick O_2 respiration, or nitrogenase synthesis

and turnover maximization (Stein & Klotz, 2016). N fixation produces ammonium (NH_4^+) that is absorbed into biomass or respired further by aerobic and anaerobic NH_3-oxidising microorganisms such as *Nitrosomonas and Nitrosococcus* (Kowalchuk & Stephen, 2001). The conversion of atmospheric nitrogen to reactive N (such as NH_4^+) always occurs by lightning, supplying reactive N to the land and ocean (Takai, 2019).

Artificial, chemical N fixation is used for producing fertilizer, explosives, and other products. The Haber-Bosch process is the most used technique to produce reactive N, mostly artificial NH_3 (Appl, 2006). Under high temperatures and pressures, the process transforms atmospheric nitrogen to NH_3 via a reaction with hydrogen (H_2). This reaction is more favorable at lower temperatures and higher pressures because it is partially exothermic (Clark, 2013). By steam reforming, hydrogen is created, followed by an iterative closed cycle in which hydrogen reacts with N to produce NH_3.

1.1.3. Nitrification

Nitrification converts NH_3 to nitrite (NO_2^-) and then to NO_3^-. It typically occurs in the soil. The bulk of nitrification occurs aerobically and is solely performed by prokaryotes. Nitrification happens in two phases, each carried out by distinct microbial populations (Kendall et al., 2007). In the initial stage, NH_3 is oxidized to NO_2^-, primarily by NH_3-oxidising bacteria or archaea (Kendall et al., 2007). Using two different enzymes, namely ammonia monooxygenase and hydroxylamine oxidoreductase, aerobic NH_3 oxidizers convert NH_3 to NO_2^- via the intermediate hydroxylamine (Takai,2019). The second stage of nitrification is the oxidation of NO_2^- to NO_3^-. This step is carried out by a subset of prokaryotes known as NO_2^- oxidizing bacteria (Ward,1996). Complete nitrification requires both NH_3 and NO_2^- oxidation.

Previously, nitrification was considered to only occur under aerobic settings. However, a novel type of NH_3 oxidation happening under anoxic conditions was recently found (Strous et al., 1999). Prokaryotes from the Bacteria phylum *Planctomycetes* perform Anammox (anaerobic ammonia oxidation) to generate energy (Strous et al., 1999)**.** Anammox bacteria were first observed in anoxic bioreactors of wastewater treatment facilities (Kuypers et al., 2005). They have now been reported in a wide range of aquatic systems, including low-oxygen zones of the ocean, coastal and estuary sediments, mangroves, and freshwater lakes (Kuypers et al., 2005). According to Kuypers et al. (2005), the anammox mechanism is thought to be responsible for a significant N loss in some parts of the ocean.

1.1.4. Assimilation

During assimilation, plants, algae, and microbes absorb NO_3^- and NH_4^+ into their biomass (Morot-Gaudry, 2001). NO_3^- is often more prevalent than NH_4^+ in non-acidic soils (Morot-Gaudry, 2001). The amount of NO_3^- and NH_4^+ absorbed varies according to plant type and climatic circumstances (Morot-Gaudry, 2001). Most absorbed NO_3^- is converted to NH_4^+ in roots and leaves and enters metabolic pathways, supporting the production of amino acids and proteins (Morot-Gaudry, 2001). Although plants cannot directly fix atmosphere N, several plant species are colonized by molecular N-fixing bacteria found in nodules on their roots (Morot-Gaudry, 2001). These bacteria convert nitrogen gas into NH_3, which plants use to meet their N requirements. In exchange, plants provide the bacteria's carbon needs (Morot-Gaudry, 2001).

1.1.5 Denitrification

Denitrification is the anaerobic conversion of NO_2^-, nitric oxide (NO), and nitrous oxide (N_2O) to nitrogen gas (Stein &Klotz, 2016). Denitrification is done by denitrifying bacteria such as *Bacillus and Pseudomonas* (Ambus & Zechmeister-Boltenstern, 2007). There is emerging evidence that certain eukaryotes may also denitrify (Risgaard-Petersen et al., 2006**).** Denitrification mainly occurs in soils, groundwater, wetlands, poorly ventilated ocean corners, and seabed sediments (Baker et al., 2000; Seitzinger, 1988). Denitrification in wastewater treatment is critical in eliminating undesired nitrates from wastewater effluent, lowering the likelihood that water released from treatment facilities would have undesirable outcomes such as algal blooms (Munch & Velthof, 2007).

Denitrification can also occur in oxic conditions. Denitrifier activity is highest in the intertidal zones, where tide cycles induce changes in oxygen content in sandy coastal sediments (Marchant et al., 2017). For example, the bacterial species *Paracoccus denitrificans* may denitrify in both oxic and anoxic conditions at the same time (Qu et al., 2016). When exposed to oxygen, the bacteria can use nitrous oxide reductase, an enzyme catalyzing denitrification's last step (Qu et al., 2016).

1.2 Stable Isotopes

Isotopes are atoms with the same number of electrons and protons but vary in neutron count (Sulzman, 2007). Stable isotopes are not radioactive, meaning they do not decay and are energetically stable (Sulzman, 2007). An *isotope* is defined as stable when the neutrons (N_*) and the protons (Z) have similar number counts ($N_*/Z \leq 1.5$) (Sulzman, 2007). Determining stable isotopes has become an essential tool for comprehensively investigating NO_3^- in groundwater

bodies. Rather than referring to the slight difference in stable isotope fractional abundances or ratios, scientists commonly use the delta notation (δ) because it provides a more convenient value to assess small changes in stable isotope distributions; the values are expressed in per mille (‰) (Sulzman, 2007):

$$\delta\ (‰) = (\frac{R_{sample}}{R_{standard}} - 1) \times 1000 \qquad (1)$$

R is the ratio of heavy-to-light isotope, R_{sample} is the ratio in the sample, and $R_{standard}$ is the ratio in the reference standard (Sulzman, 2007).

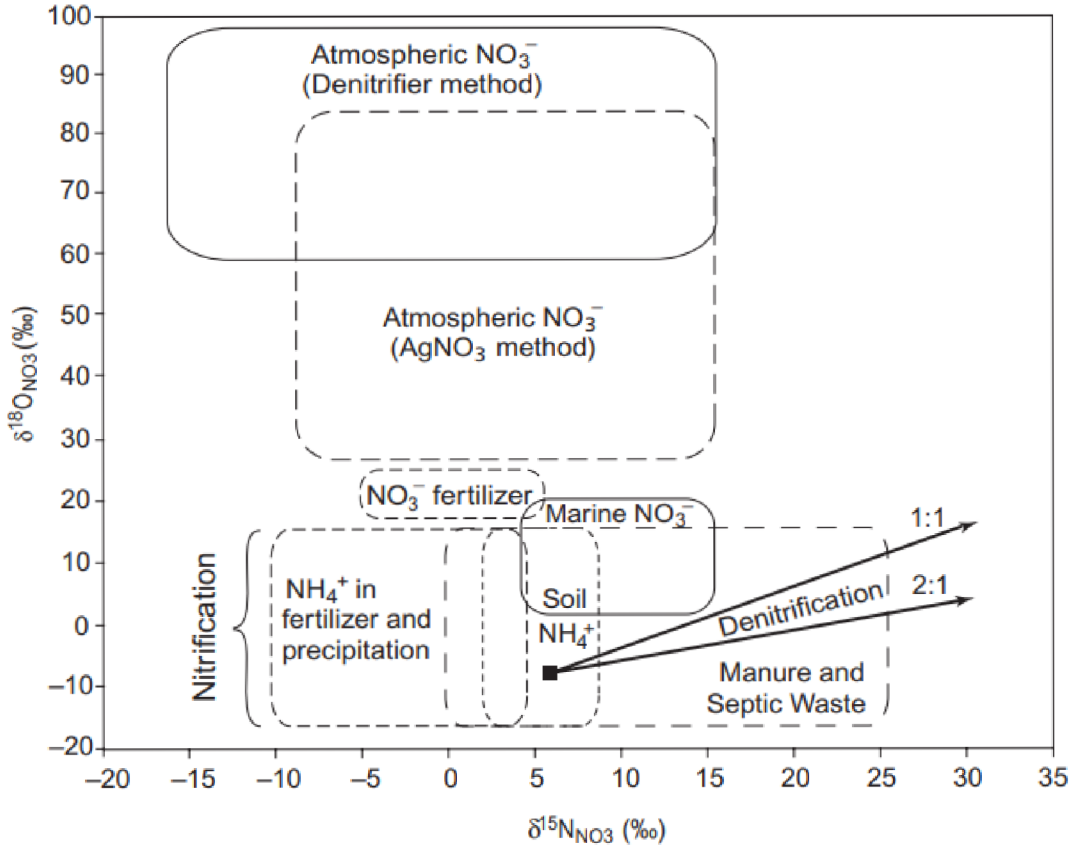

Figure 2: "Kendall plot" from Kendall et al. (2007). This figure shows typical values of $\delta^{15}N$ and $\delta^{18}O$ of NO_3^- from various N sources. The arrows indicate systematic changes in δ values of NO_3^- when it is a substrate for denitrification.

After determining the δ values of NO_3^-, the source of NO_3^- can be inferred using the so-called "*Kendall plot*" (Fig. 2). $\delta^{18}O$-NO_3^- values from -20 ‰ to +15 ‰ signify nitrification, while $\delta^{15}N$-

NO_3^- values within -10 ‰ to +25 ‰ signify the processes, nitrification, and denitrification. $\delta^{18}O$-NO_3^- values mark atmospheric deposition ranging from +30 ‰ to +100 ‰ (Kendall, 2007).

1.2.1. Isotope effects

Because stable isotopes of the same element have the same proton and electron shells, they undergo the same chemical reactions (Sulzman, 2007). Nonetheless, the atom with more neutrons is heavier than the typically more abundant atom with fewer neutrons (Sulzman, 2007). Therefore, 'heavy' isotopes typically react slower than 'light' isotopes, which react faster (Sulzman, 2007). In other words, physical and chemical processes "prefer" the lighter isotope and "discriminate" against the heavier isotope (Sulzman, 2007). This mass discrimination is also called fractionation and can be measured to reveal processes in biogeochemical systems (Sulzman, 2007). Without fractionation, there would be a uniform distribution of isotopes across all N species in the environment (Sulzman, 2007). Scientists can identify processes from observed isotope distributions and the underlying fractionation patterns. These patterns generated from specific processes are referred to as isotope effects (Sulzman, 2007).

When an equilibrium reaction may be reversible, equilibrium isotope effects occur (Sulzman, 2007). Equilibrium fractionation reactions occur when the isotope distribution changes across chemical substances or phases during a reaction (Sulzman, 2007). Back reactions and chemical equilibrium can occur in these reactions because the reactants and products remain in close contact in a closed, well-mixed system (Sulzman, 2007). Although the reactants and products are identical in equilibrium reactions, their end masses differ from their beginning masses (Sulzman, 2007). The magnitude of the mass difference varies with temperature, with the most considerable differences occurring at the lowest temperatures (Sulzman, 2007). In equilibrium exchange reactions, the heavier isotope is likely found where bonds are strong (Sulzman, 2007). Kinetic isotope effects, conversely, occur in irreversible or unidirectional processes when the reverse reaction is blocked or does not occur (Sulzman, 2007). Kinetic fractionations are considerably higher than equilibrium fractionation factor, and result in the lighter isotope amassing in the product (lighter moves quicker) (Sulzman, 2007). For N cycle processes, kinetic isotope fractionation is often the most relevant (Sulzman, 2007).

To describe isotope effects, fractionation factors α (ratios of two isotope ratios) are used:

$$\alpha_{ps} = R_P / R_s \quad (2)$$

R is the heavy-to-light isotope ratio in the immediate product (Rp) and substrate (Rs). Subscripts may indicate the phase rather than which side of the reaction a chemical is mentioned in equilibrium exchange reactions (Sulzman, 2007). Except for hydrogen isotopes, for which α values can be as high as four at ambient temperature (Kendall & Caldwell, 1998), α values are typically close to 1.00. If an α value is greater than one, the instantaneous product is more enriched in the heavier isotope than the substrate (Sulzman, 2007).

The isotopic composition of two substances and its fractionation factors are related according to:

$$\alpha_{A-B} = (1000 + \delta_A)/(1000 + \delta_B) \quad (3)$$

A and B represent different substances. α values are generally small; therefore, authors frequently report the deviation of the fractionation factor from unity using ε (Sulzman, 2007):

$$\varepsilon_{A-B} = (\alpha_{A-B} - 1) \times 1000 \quad (4)$$

ε is referred to as enrichment (when ε is greater than 0) or depletion (when ε is less than 0) of the heavy isotope in compound B to compound A (Sulzman,2007).

Another common term used to describe isotope effect is "discrimination". Discrimination is the degree to which any process avoids the heavy isotope. One formula used to calculate discrimination is (Sulzman, 2007):

$$\Delta_{A-B} = \delta_A - \delta_B \quad (5)$$

1.2.2. Stable isotope analysis

J. Thompson developed isotope ratio mass spectrometry (IRMS) in 1910 to measure stable isotope ratios. A mass spectrometer is used in to separate charged atoms or molecules depending on their mass-to-charge ratio (m/z) (Sulzman, 2007). Dual-inlet (DI-IRMS) and continuous flow (CF-IRMS) are the primary types; In DI-IRMS, the analyte must be a gas (Sulzman, 2007). CF-IRMS may analyze dissolved molecules, atmospheric air, soil, or leaves, gathering isotopic data for particular elements or compounds in the mixture (Sulzman, 2007). The IRMS comprises four major parts: an intake system, an ion source, a mass analyzer, and an ion detector (Fig. 3). The main difference between CF and DI systems lies in their intake component. The inlet system's crucial aspect is using capillary tubes to prevent isotope separation during gas input (Sulzman, 2007).

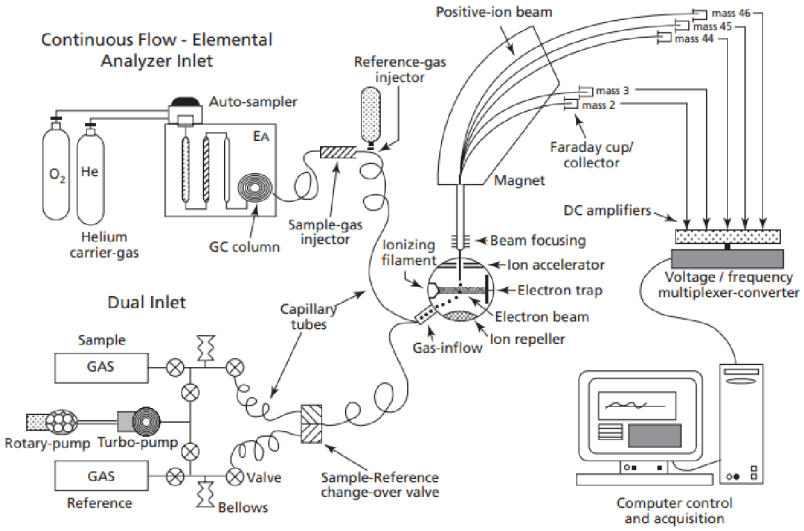

Figure 3: From Dawson & Brooks (2001). A diagram showing the continuous flow (top) and dual inlet (bottom) interfaces to an isotope ratio mass spectrometer's ion source (center). Ionized gases exiting the ionization chamber are accelerated and focused (by the magnet) towards the collector array.

The ion beam undergoes bending in the mass analyzer due to a magnetic field, with heavier isotopes bending less than lighter ones. The system's flat-topped ion beams ensure optimal capture in specialized Faraday cups in the ion detector. These cups, connected to a computer, translate relative signal intensity into isotope ratios expressed as an δ value in parts per thousand compared to a standard (Suzman, 2007). This method, detailed by Sulzman (2007) has revolutionized stable isotope ratio analysis, thus allowing precise measurement and analysis across various scientific fields.

1.2.3. Stable Nitrate Isotopes

NO_3^- consists of nitrogen and oxygen isotopes. ^{14}N and ^{15}N are the two stable isotopes of nitrogen, with 99.64% and 0.35% relative abundances in nature, respectively (Ostrom & Ostrom, 2006). Oxygen, on the other hand, exists naturally in three stable isotopes: ^{16}O, ^{17}O, and ^{18}O. The most prevalent stable O isotope on Earth is ^{16}O, which accounts for 99.757% of all atoms, whereas ^{17}O (0.038%) and ^{18}O (0.205%) are found in far lower proportions across the planet (Wright, 2016).

1.2.4 Previously used methods used for stable nitrate isotope analysis.

One of the previously used methods for NO_3^- analysis was the elemental analyzer method, which requires the production of NO_3^- salt. This method has been used frequently due to its cost-effectiveness. Even with this, some researchers are apprehensive that this may pose a risk to their investigations, as such services may not provide accurate and precise results (Kuveke et al., 2022).

Another method was the bacterial denitrifier method. This approach is based on the isotopic measurement of N_2O produced by denitrifying bacteria lacking nitrous oxide - reductase activity from NO_3^-, therefore, the isotopic compositions of nitrogen and oxygen from NO_3^- are accessible (Sigman et al., 2001). This method, nevertheless, is time-consuming and requires biological expertise, which relies on sterile lab techniques, microbial manipulation, and cultivation.

The Cadmium-azide reduction method was also used previously. This technique includes reducing NO_3^- to NO_2^- with porous cadmium and then to N_2O with sodium azide in an acetic acid buffer (McIlvin & Altabet, 2005). However, this approach may be time-consuming since only 15 samples can be analyzed daily. Moreover, it is a sequential method with a robustness test at each step. Altabet et al. (2019) state that both the bacterial method and the cadmium-azide method require complicated, laborious chemical reactions and use of toxic reagents for the conversion of nitrate to N_2O. On the other hand, a new titanium (III) reduction method for NO_3^- isotope analysis was recently developed by Altabet et al. (2019) and the International Atomic Energy Agency (IAEA). It has the advantages of low cost, simplicity, and the absence of harmful chemicals or need to maintain anaerobic bacterial cultures. The titanium (III) approach is simple to implement in laboratories with nitrous oxide headspace sampling apparatus.

2 Thesis aim

This study aims to develop and install protocols to track nitrate isotopes to constrain the relative inputs and processes (e.g., nitrification and denitrification) occurring in the pristine Plešné, Čertovo, and Černé Lakes in the Bohemian National Forest in Czech Republic. Laboratory research goals include the preparation of reagents, standards and glassware, and the chemical reduction of NO_3^- to N_2O using titanium (III) chloride ($TiCl_3$) catalyst to determine stable isotope ratios of N and O in NO_3^- samples collected from July 2020 to June 2021.

3 Materials and method

As mentioned in the preceding chapter, this thesis aims to create and implement techniques for tracking nitrate isotopes in the pristine Plešné, Čertovo, and Černé Lakes of the Bohemian National Forest in Czech Republic. This chapter thoroughly explains all materials and the measurement method utilized to analyze nitrate isotopes in collected samples to accomplish these goals. This chapter serves as a step-by-step guide for putting the protocols produced in the thesis goal into action, allowing a smooth transition from the theoretical framework to the actual implementation of the study.

3.1 Materials

All essential equipment, materials, and chemicals used during the experiment are listed (after IAEA protocol; L. Wassenaar, pers. comm. 2020).

3.1.1. Apparatus

The materials used are listed below:

1. Exetainers™ with butyl-grey septum caps (12 mL).
2. Variable-volume micro and macro pipettes with disposable plastic tips (10 mL, 5 mL, 1000 µL, 100 µL).
3. Fume hood and personal safety equipment such as gloves and eye protection.
4. Waste container for chemical disposal.
5. Appropriate beaker size, glass cover and stirrer for titanium $TiCl_3$ (30%) preconditioning.
6. Weighing scale and weighing boat to weigh the required Zinc (Zn) powder amount.
7. Glass beakers to handle standards.
8. Liquid Nitrogen (LN_2).
9. High purity Helium (He) for flushing vials.
10. Hydrogen (H_2) for flushing vials.

3.1.2 Reagents, reference material stock solutions and internal standard stock solutions.

The reagents used are as follows:

- $TiCl_3$ (30 %) in 10 % HCl (Merck P/N 8.08308.0500).
- Zn metal powder (Goodfellow ZN006040/7; 150 microns, 99.9 % purity), 200 g.
- HCl (10 % v/v). Made with degassed DI water.
- Sulfanilic acid (2.5 nM).

- Degassed deionized (DI) water.

Reference Material stock solutions:

- USGS34: 7.21 mg KNO_3 in 1 L degassed DI water (1 mg L^{-1} N / 71 µM).
- USGS32: 7.21 mg KNO_3 in 1 L degassed DI water (1 mg L^{-1} N / 71 µM).
- USGS35: 6.07 mg $NaNO_3$ in 1 L degassed DI water (1 mg L^{-1} N / 71 µM).

Internal standards stock solutions:

- KNO_3: 7.21 mg KNO_3 in 1 L degassed DI water (1 mg L^{-1} N / 71 µM).
- $NaNO_3$: 6.07 mg $NaNO_3$ in 1 L degassed DI water (1 mg L^{-1} N / 71 µM).

3.2 Conversion of nitrate into nitrous oxide by titanium(III) chloride.

Using the new $TiCl_3$ method, we adapted and tested three protocols for this thesis to convert NO_3^- to the IRMS-amenable N_2O gas (Table I). Each protocol was tested for the reaction yield (total N_2O signal) and the converted nitrate's precision of $\delta^{15}N$ and $\delta^{18}O$ values. The first was the protocol Altabet et al. (2019) described which the International Atomic Energy Agency (IAEA) implements to monitor nitrate isotopes worldwide. The second was an unpublished adaptation of this protocol developed by colleagues (Li et al., 2019) at Purdue University (Lafayette, Indiana, USA), who use lower amounts of $TiCl_3$ and claim to achieve higher reaction yield. The final was an experimental protocol that sought to enhance the reaction efficiency by adding He + H_2 gas to the headspace of the reaction vial. The three protocols differed in the relative ratios of $TiCl_3$ reagent to the sample, the gas composition of the headspace during conversion, and/or in the order in which the various reaction components were added to the vials.

Table I: Description of protocols adapted and implemented for this thesis.

Protocol	Adapted IAEA	Purdue	He+H_2
Sample volume (mL)	3	2	3
[NO_3^--N] (ppm)	0.2	0.2	0.2
$TiCl_3$ reagent (%, w/v)	30 %	0.24 %	30 %
Amount $TiCl_3$ (mL)	0.15	1	0.15
Final $TiCl_3$ concentration (% w/v)	1.4 %	0.08 %	1.4 %
Amount of Titanium (mol)	237	13	237
Amount N (nmol)	43	14	43
Titanium sample ratio (TSR, mol)	5.5	0.9	5.5
Headspace volume (mL)	9	9	9
Headspace composition	air	He	He + 1 % H_2
Reaction time (~hours)	18	18	18

For the adapted IAEA protocol, 3 mL of each internal standard was pipetted into vials (12 mL), then 150 µL of preconditioned $TiCl_3$ was pipetted into the vial and immediately sealed with the septum cap. The preconditioning of $TiCl_3$ was carried out in the fume hood since the reaction is exothermic, producing H_2 gas approximately 30 minutes before use to ensure the efficacy of the $TiCl_3$-reducing reagent by removing Ti (IV). For preconditioning, 1 g of Zn metal powder was weighed and slowly added to 10 mL 30 % $TiCl_3$. Afterwards, the beaker was covered with a watch glass cover to prevent splatter. After the initial reaction had subsided, the solution was gently stirred with a glass stir-stick. The reaction was complete after 30 min when there were no more bubbles and the mixture had cooled to room temperature. The supernatant was collected with a micro-pipette to prevent bringing Zn metal and precipitate from the bottom of the beaker. The original $TiCl_3$ reagent bottle was flushed with argon gas and carefully sealed with parafilm after use to minimize oxidation or water absorption. Preconditioned $TiCl_3$ reagent that had not been utilized was disposed of as chemical waste. This procedure was also repeated for the addition of preconditioned $TiCl_3$ to international reference standards. Lastly, all the vials were shaken overnight for ~18 hours to complete the reduction of NO_3^- into N_2O.

For the Purdue protocol, 0.4 mL of 30 % $TiCl_3$ was diluted with 49.6 mL deionized water. The solution was poured into a 100 mL stoppered bottle and sealed for preconditioning. Then, the bottle's headspace was flushed with helium for 2 minutes to remove air. Then, the bottle was placed on the shaker for 2 hours to remove oxygen or other oxidants from the reducing solution. Afterwards, the headspace was flushed with helium for 2 minutes more. Then, 12 mL exetainer vials were flushed with helium for 6 minutes. Then, 2 mL of the NO_3^- standard was injected through the septa. Afterwards, 1 mL of the conditioned $TiCl_3$ solution was injected through the septa. This step was also repeated for the reference standards. Lastly, all the vials were shaken overnight for ~ 18 hours to complete the reduction of NO_3^- into N_2O.

For the He + H_2 protocol, 150 µL of preconditioned 30 % $TiCl_3$ was pipetted into each vial (12 mL), which was then immediately sealed with septum caps to avoid oxidation. The vials were flushed with helium containing 1 % (v/v) H_2 for 10 minutes. Afterwards, the vials were shaken for 20 minutes. Then, 3 mL of each standard was injected into each vial through the septa. This was also repeated for the international references. Lastly, all the vials were shaken overnight for ~ 18 hours to complete the reduction of NO_3^- into N_2O.

3.3 Stable isotope analysis of nitrous oxide converted from nitrate.

After the reduction procedure, the vials were introduced to the IRMS instrument for analysis. The analysis was achieved with a GasBench II peripheral interfaced with a MAT 253 Plus IRMS via a Conflo IV interface (Thermo Scientific, Bremen, Germany). The headspace of the exetainer was sampled by a double-holed needle using a CTC PAL autosampler and the flush-fill line of the GasBench device. The flush rate was ca. 25 mL $min^{-1,}$ and the flush time was 5.5 min. The headspace sample was passed through a magnesium perchlorate and ascarite trap to remove water and CO_2, respectively, then collected in a sample loop (50 cm PoraPlot Q; ø = 0.53 mm; Restek) submersed in LN_2. N_2O in the sample was then separated from CO_2 and other gases by injecting onto a Carboxen 1010 PLOT column (30 m × 0.53 mm, 30 µm film thickness, Supelco; temp = 90 °C, flow rate 2.6 mL min^{-1}) with He as the carrier gas. The sample was then introduced to a MAT 253PLUS IRMS via the CF interface. $\delta^{15}N$ and $\delta^{18}O$ values were determined relative to an N_2O working gas and then corrected for linearity according to the peak height relationship and titanium-to-sample ratio (Altabet et al., 2019). The corrected values were then normalized to the $\delta^{15}N$ Air and $\delta^{18}O$ VSMOW scales via the concurrent analysis of USGS32, USGS34, and USGS35 international standards.

3.4 Sample preparation and nitrate concentration analysis.

Samples for this thesis were collected from Plešné, Čertovo and Černé lakes in 3-week intervals from June 2020 to July 2021. The study of Kopáček et al. (2006) and Lukavský (2009) offers a description of the lakes. The samples were collected from the lake surface and specific inlet and outlet tributaries. Samples were filtered through 0.45 µm GF/F filters. To preserve the samples, 1 mL of 2.5 nM sulfanilic acid in 10 % HCl was added to each 100 mL of filtered water sample to reduce the pH to 2-3; HCl could keep the samples for several months. Sulfanilic acid binds with NO_2^-, so only NO_3^- will be reduced to N_2O with the $TiCl_3$ treatment. NO_3^- concentration were measured by ion chromatography for all samples, and data were kindly provided by P. Porcal (Institute of Hydrobiology, BC-CAS, Ceske Budejovice, Czechia). For NO_3^- isotope analysis, samples were diluted to NO_3^--N concentration of 0.2 ppm.

4 Results

The N and O stable isotope ratios of NO_3^-, as measured by the chemical reduction of NO_3^- to N_2O using a $TiCl_3$ catalyst, are detailed in this section. The findings related to environmental samples are a direct outcome of the adapted IAEA approach used, and they help to demonstrate the efficacy of the procedure employed for this study. The IRMS was under repair for several months in 2021, during the months devoted to my thesis experiments, hindering NO_3^- analyses and data acquisition for this thesis. When the IRMS was fixed in November 2021, the lake samples collected for this thesis were analyzed by the IRMS operator using the method I helped install in the lab; however, data are unavailable for all sampling days and locations. This also explains why data from 2022 are also presented from some of the Lakes. For some samples, NO_3^--N levels were below the detection limit of the IRMS method.

4.1 Comparison of nitrous oxide conversion for analysis of nitrate standards.

The peak for N_2O (Fig. 4) was described by peak amplitude (Ampl 44), area (Area All, including the peaks for masses 44, 45, and 46), and the precision of the isotope measurements (δ values) was calculated for four replicate samples, which are summarized in Table II. The adapted IAEA method generally gave higher "Ampl 44" and "Area All" than the other two methods. The precision of the δ values varied considerably within and between methods, which were tested for a range of nitrate concentrations. Tests with higher NO_3^--N concentrations (> 1ppm) generally had a higher standard deviation of δ values and were less precise. The coefficient of variation of "Ampl 44" and "Area All" was also above 25 % for when NO_3^--N levels were above >1 ppm, and <10 % when NO_3^--N was below 0.5 ppm.

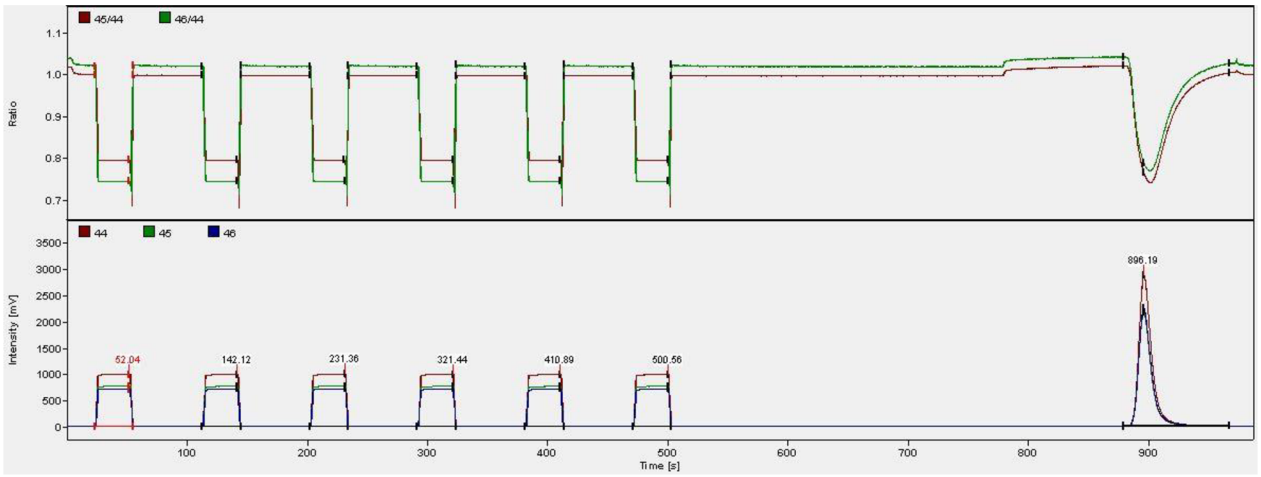

Figure 4: Example of an isotope ratio (upper) and mass trace chromatogram (lower) of N_2O converted from an in-house potassium nitrate standard and detected by the IRMS. The first six box-shaped peaks are pulses of the N_2O working gas; the peak on the far right is N_2O converted from NO_3^-.

Table II: Calculated averages and standard deviations for the internal standards ranging from 0.1 to 1 ppm. For each value shown, n = 4. The rows highlighted in grey indicate the best performance based on evaluation criteria.

			AVG	SD	AVG	SD	SD	SD
Identifier	NO_3^--N (ppm)	Method	Ampl 44	Ampl 44	Area All	Area All	$\delta^{15}N/^{14}N$	$\delta^{18}O/^{16}O$
$NaNO_3$	0.1	Adapted IAEA	479	43	5.5	0.5	1.5	1.2
$NaNO_3$	0.1	Purdue	173	12	2.1	0.2	0.2	1.4
$NaNO_3$	0.1	He + H_2	134	5	1.6	0.1	0.6	9.6
KNO_3	0.1	Adapted IAEA	532	41	6.1	0.4	0.6	0.8
KNO_3	0.1	Purdue	109	6	1.3	0.1	0.8	5.1
KNO_3	0.1	He + H_2	135	13	1.6	0.2	0.0	1.0
$NaNO_3$	0.2	Adapted IAEA	**1127**	**92**	**13.1**	**1.1**	**0.1**	**0.7**
$NaNO_3$	0.2	Purdue	909	36	10.7	0.5	1.0	0.9
$NaNO_3$	0.2	He + H_2	923	31	10.8	0.4	0.5	1.9
KNO_3	0.2	Adapted IAEA	**1187**	**67**	**13.8**	**0.8**	**0.2**	**0.6**
KNO_3	0.2	Purdue	877	74	10.2	0.8	1.1	0.9
KNO_3	0.2	He + H_2	863	24	10.0	0.4	0.6	0.2
$NaNO_3$	0.5	Adapted IAEA	1541	381	30.6	7.9	2.9	1.5
$NaNO_3$	0.5	Purdue	747	14	9.2	0.3	0.03	0.77
$NaNO_3$	0.5	He + H_2	651	18	8.0	0.3	0.13	0.50
KNO_3	0.5	Adapted IAEA	1095	592	21.0	11.8	5.5	7.1
KNO_3	0.5	Purdue	580	47	7.1	0.6	1.81	5.46
KNO_3	0.5	He + H_2	696	76	8.5	0.9	0.02	1.16
$NaNO_3$	1.0	Adapted IAEA	2520	1178	50.2	24.1	3.9	4.4
$NaNO_3$	1.0	Purdue	1002	140	12.3	1.7	2.7	9.6
$NaNO_3$	1.0	He + H_2	858	25	10.6	0.3	0.3	0.7
KNO_3	1.0	IAEA	2778	1289	55.7	26.3	3.3	4.4
KNO_3	1.0	Purdue	640	83	7.8	1.0	0.4	0.1
KNO_3	1.0	He + H_2	791	40	9.7	0.4	0.3	0.1

The final protocol selected for nitrate isotope analysis was the adapted IAEA method, which was the simplest in terms of sample handling, yielded the highest N_2O peak, and exhibited the best precision. Measurement uncertainty (± one standard deviation of the mean) determined for in-house standards was < 0.2 ‰ and 0.7 ‰ for $\delta^{15}N$ and $\delta^{18}O$, respectively, at 0.2 ppm (Table II). A template

designed for diluting samples and the addition of $TiCl_3$ is given in Appendix 1: Sequence template for 200ppb NO_3^--N analysis.

4.2 Nitrate isotope analysis of natural lake samples.

Samples were obtained from various sampling sites throughout the year's four seasons. Most of the analyzed samples came from Plešné Lake. The subsequent results are outlined below:

4.2.1. Plešné Lake

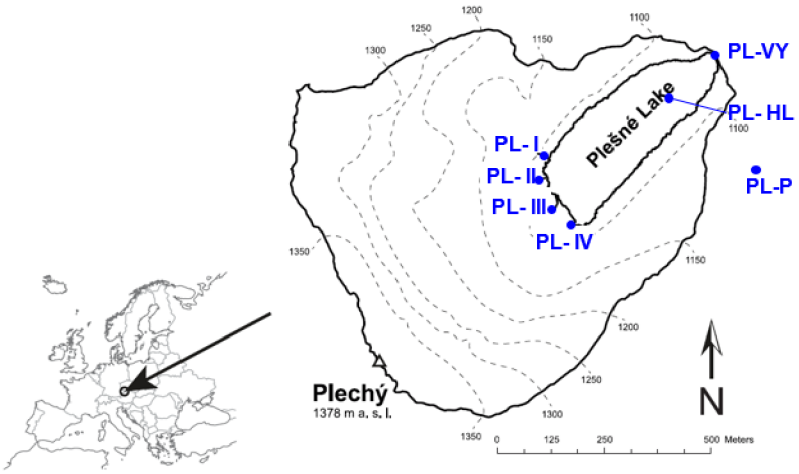

Figure 5: Adopted from Porcal et al. (2014) This figure shows the watershed of Plešné Lake, its location in Europe and the sampling locations. PL-I to PL-IV are the lake tributaries, PL-VY is the lake outlet, PL-HL is surface waters, and PL-P is an open area precipitation plot. Samples were collected from all collection sites.

4.2.1.1.Plešné NO_3^--N concentration.

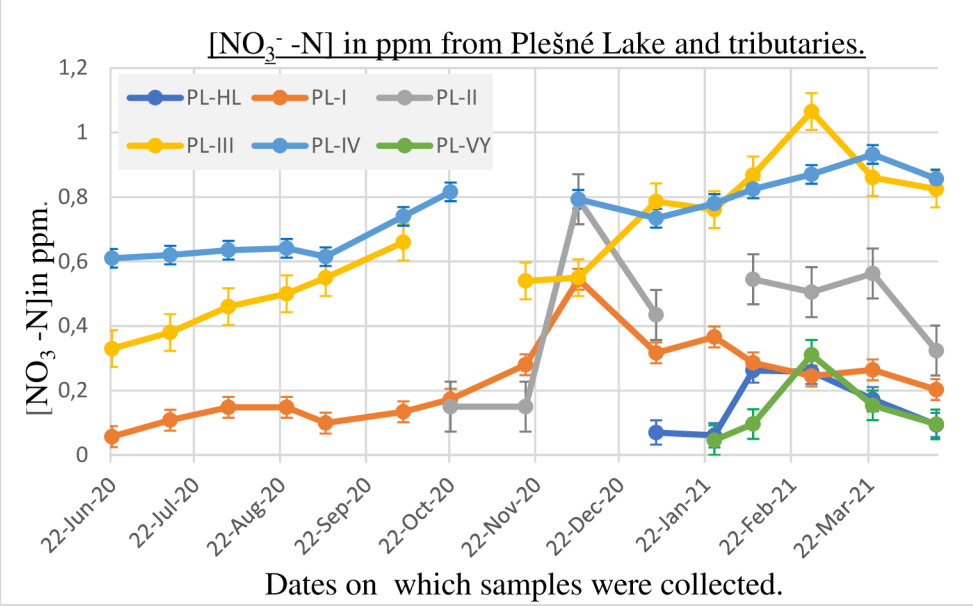

Figure 6: NO_3^--N concentrations from Plešné Lake tributaries over time.

Samples collected from the lake's surface (PL-HL) exhibited a concentration range of 0.07 ppm to 0.262 ppm. There was no seasonal variation observed. Samples taken from PL-I indicated unique seasonal concentration fluctuations. Concentrations throughout the summer varied from 0.08 ppm to 0.16 ppm. By the end of the summer, the concentration had dropped from 0.16 ppm to 0.12 ppm. Then, concentrations progressively increased from 0.12 ppm to 0.52 ppm in fall. However, the values varied between 0.52 ppm and 0.28 ppm from the end of fall through winter. There was a subsequent decline from 0.28 ppm to 0.2 ppm in spring. Samples collected from PL-II exhibited seasonal fluctuations within the concentration range of 0.2 ppm to 0.8 ppm. The concentration reached its highest in winter from 0.2 ppm to 0.8 ppm. Between summer and mid-fall (22nd June 2020 to mid-October 2020), PL-III samples exhibited a linear concentration rise from 0.32 ppm to 0.66 ppm. The highest concentration was recorded in spring, which was 1.1 ppm. Lake samples obtained in the summer from PL-IV showed little to no increase in their concentration. Concentrations varied from 0.68 ppm to 0.80 ppm during fall (from 22nd September to 22nd November 2020). Winter concentrations ranged between 0.76 ppm and 0.92 ppm (December 2020 to February 2021). Notably, concentrations began to fall from their peak of 0.92 ppm in the spring, reaching 0.84 ppm. The concentration of samples from PL-VY peaked at 0.32 ppm towards the

end of winter from 0.04 ppm; yet, the concentration had declined rapidly to 0.16 ppm by mid-March. Precipitation samples (PL-P) ranged in NO_3^--N from 0.05 to 0.54 ppm.

4.2.1.2.Plešné NO_3^- isotopes.

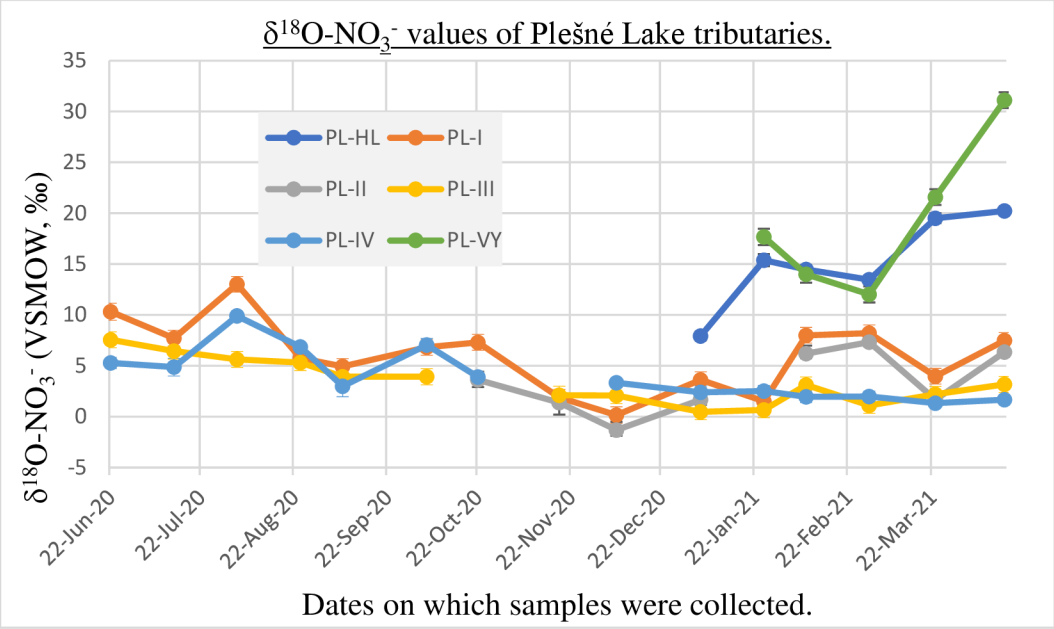

Figure 7: $\delta^{18}O\text{-}NO_3^-$ in Plešné Lake and its tributaries.

Plesne lake tributaries generally exhibited a gradual decrease in $\delta^{18}O\text{-}NO_3^-$ values (~5-10 ‰) from spring to winter (Fig. 7). Samples from PL-I have positive $\delta^{18}O\text{-}NO_3^-$ values, ranging from 0 ‰ to 13 ‰. Notably, during the summer period, specifically from 22nd July 2020 to early August 2020, these samples reached their highest $\delta^{18}O\text{-}NO_3^-$ value of 13 ‰. For samples from PL-II, the $\delta^{18}O\text{-}NO_3^-$ values varied between -1‰ and +7 ‰. From mid-fall to early winter (22nd October 2020 to mid-December 2020), there is a linear decline in the $\delta^{18}O\text{-}NO_3^-$ value from 3.9 ‰ to -1 ‰, followed by a subsequent rise for the remainder of the winter into spring. Samples from PL-III all demonstrate positive $\delta^{18}O\text{-}NO_3^-$ values ranging from 0.5 ‰ to 7.6 ‰. Likewise, samples collected from PL-IV consistently show positive $\delta^{18}O\text{-}NO_3^-$ values ranging from 1‰ to 10 ‰. The samples gathered from PL-HL throughout winter and spring always exhibit positive $\delta^{18}O\text{-}NO_3^-$ values ranging from 7 ‰ to 20 ‰. Samples obtained from PL-VY display positive $\delta^{18}O\text{-}NO_3^-$ values ranging from 12 ‰ to 31 ‰, indicating enrichment in ^{18}O relative to the tributaries and similar to PL-HL. Notably, these values demonstrate a linear increase from the end of winter into spring, reaching their peak of 31 ‰ in April 2021.

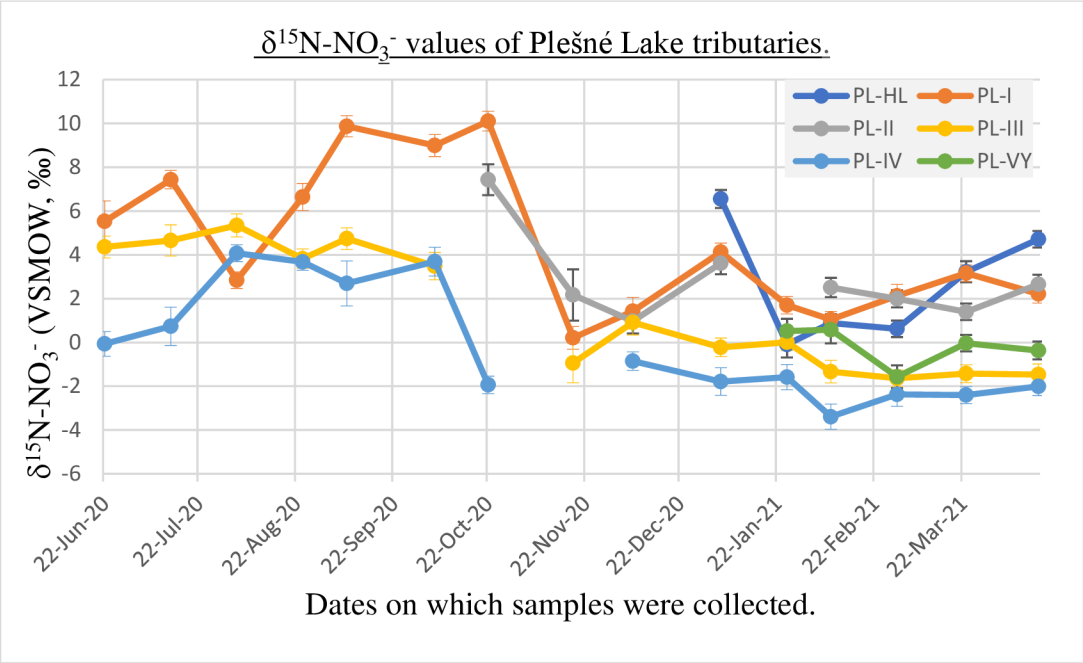

Figure 8: shows the δ values of $^{15}N\text{-}NO_3^-$ in the Plešné Lake and tributaries.

Fig. 8 illustrates the variability in $\delta^{15}N\text{-}NO_3^-$ values within samples gathered from PL-HL, ranging widely from -0.1 ‰ to 6.6 ‰. Between 22nd December 2020 and 22nd January 2021, a decrease in $\delta^{18}O\text{-}NO_3^-$ values was observed, followed by a rise from -0.1 ‰ to 4.8 ‰ extending into the spring. Regarding PL-I, Fig. 8 also depicts fluctuations in $\delta^{18}O\text{-}NO_3^-$ values from 0.2 ‰ to 10.1 ‰. Notably, the sample obtained on 22nd October 2020 displayed the highest $\delta^{18}O\text{-}NO_3^-$ value of 10.1 ‰. In contrast, the sample from 22nd November 2020 recorded a $\delta^{18}O\text{-}NO_3^-$ value of 0.1 ‰, indicating a substantial drop from the previously measured October sample. The PL-II samples displayed a similar fluctuating trend. Samples obtained during the fall depicted a decrease in their $\delta^{18}O\text{-}NO_3^-$ values, ranging from 7.2 ‰ to 2.2 ‰. Winter-collected samples showed $\delta^{18}O\text{-}NO_3^-$ values between 1‰ and 3.6 ‰, while spring samples varied from 1.4 ‰ to 2.7 ‰. Generally, the samples collected from PL-II consistently exhibited positive $\delta^{18}O\text{-}NO_3^-$. Samples obtained from PL-III exhibited no consistent pattern. Those gathered during the summer had $\delta^{18}O\text{-}NO_3^-$ values ranging between 3.8 ‰ and 5.3 ‰. However, samples collected from late fall through spring had negative $\delta^{18}O\text{-}NO_3^-$. Samples collected from PL-IV during winter through spring consistently demonstrated negative $\delta^{18}O\text{-}NO_3^-$ values, ranging from -3.4 ‰ to -0.9 ‰. Samples acquired from summer through fall had $\delta^{18}O\text{-}NO_3^-$ values within the range of -2 ‰ to 4.1 ‰. This pattern suggests that during the summer until the onset of fall. Samples collected from PL-VY ranged in $\delta^{18}O\text{-}NO_3^-$ values from -1.6 ‰ to +0.5 ‰. The collected samples demonstrated positive $\delta^{18}O\text{-}NO_3^-$ values of

0.5 ‰ and 0.6 ‰ during winter. However, in spring, there was a noticeable shift toward lower $\delta^{18}O\text{-}NO_3^-$ values, ranging from -1.6 ‰ to 0 ‰.

4.2.1.3 Kendall Plot of Plešné Lake.

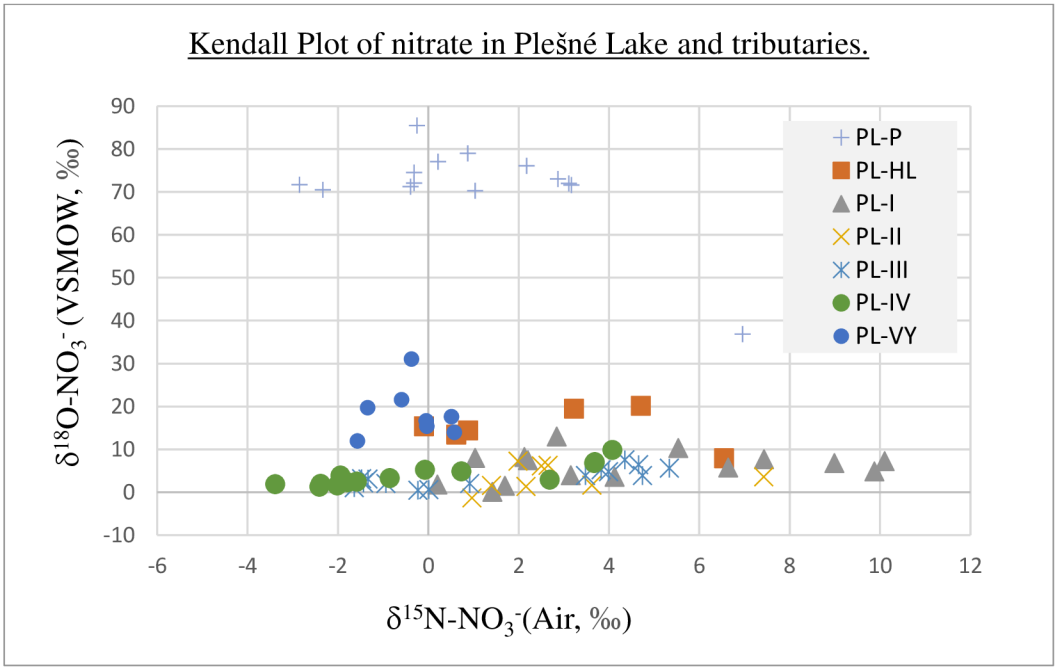

Figure 9: Kendall Plot of $\delta^{15}N\text{-}NO_3^-$ and $\delta^{18}O\text{-}NO_3^-$ values in Plešné Lake. PL-I to PL-IV are lake tributaries, PL-P is open area precipitation plot, PL-HL is surface water and PL-VY is outlet.

Fig. 9 illustrates that the tributaries displayed $\delta^{15}N\text{-}NO_3^-$ values from -4 ‰ to +10 ‰. Contrarily, samples from PL-VY exhibited a broader $\delta^{18}O\text{-}NO_3^-$ range within +10 ‰ to +30 ‰. Samples from PL-P exhibited $\delta^{15}N\text{-}NO_3^-$ values within -3 ‰. to +3.5 ‰ and a more comprehensive range of $\delta^{18}O\text{-}NO_3^-$ values within +70 ‰ to 85.5 ‰, except for one outlier (+36 ‰).

4.2.2 Čertovo

The NO_3^--N concentration measured from the tributaries ranged from 0.3 ppm to 4.8 ppm. No apparent seasonal trends in the NO_3^--N concentration in Čertovo Lake or its tributaries was observed (data not shown).

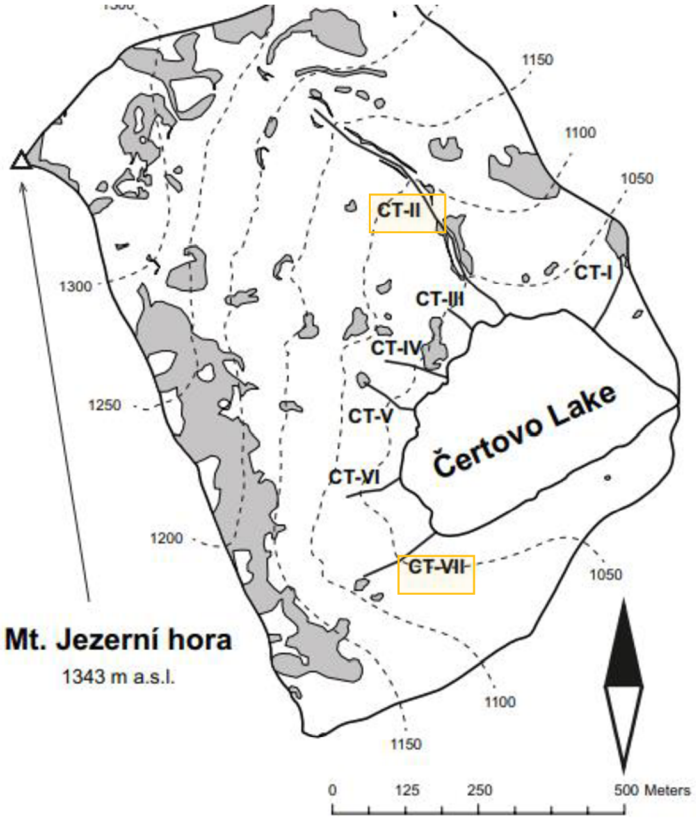

Figure 10: Adopted from Kopáček et al. (2013) This figure shows the watershed of Čertovo Lake and the sampling locations. Data presented in this thesis are limited to the tributaries CT-II and CT-VII (marked sites in orange), as explained in Section 4 above.

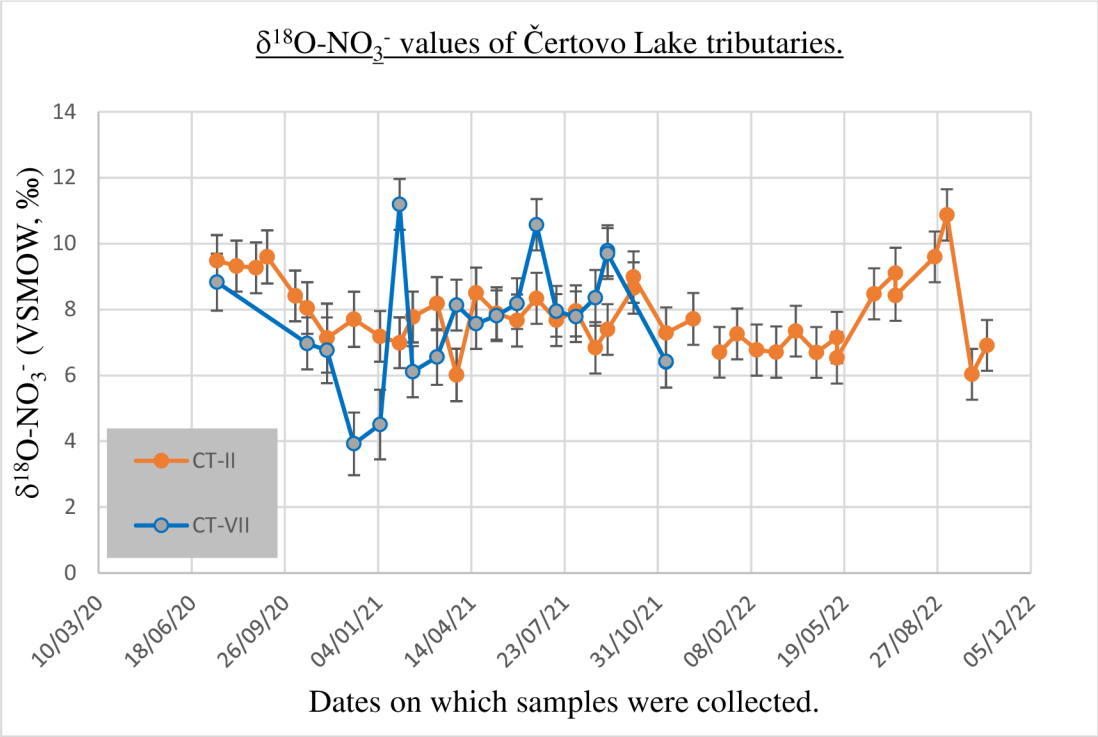

Figure 11: shows the δ values of $^{18}O\text{-}NO_3^-$ in the Čertovo Lake tributaries.

In Certovo Lake $\delta^{18}O\text{-}NO_3^-$ values were positive and fluctuated with no systematic trend across all seasons. The $\delta^{18}O$ values from CT-II ranged from +6 ‰ to +11 ‰. The highest and lowest $\delta^{18}O$ values were recorded in fall (6th September and 3rd October 2022, respectively). The $\delta^{18}O$ values from CT-VII ranged from 4 ‰ to 12 ‰.

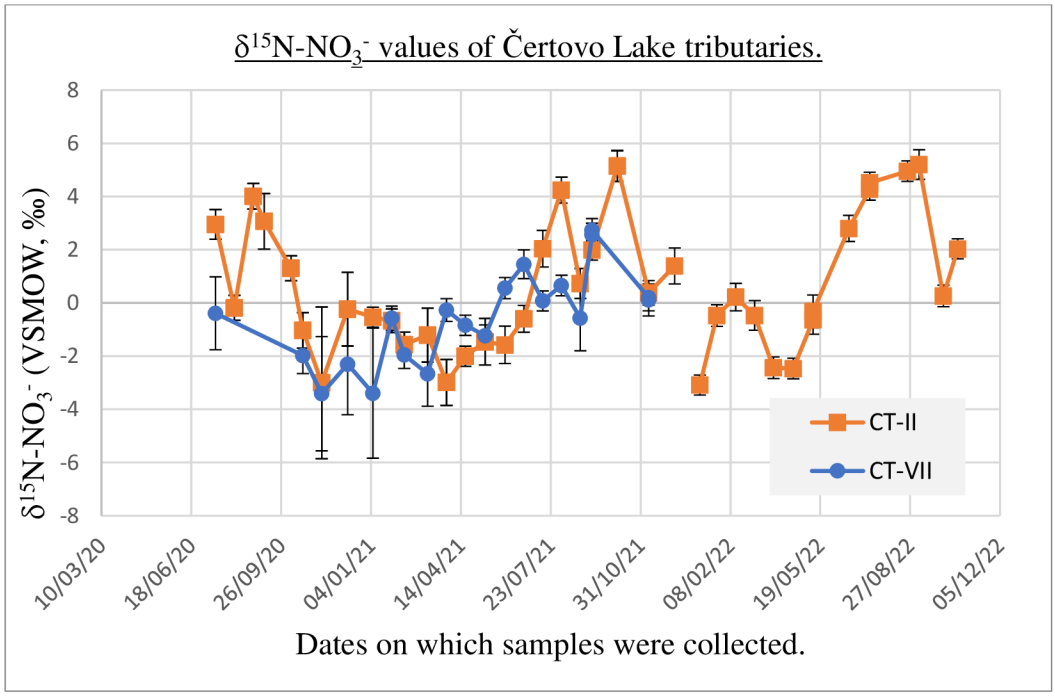

Figure 12: $\delta^{15}N\text{-}NO_3^-$ values from Čertovo Lake tributaries.

δ^{15}N-NO_3^- values in Certovo tributaries were consistently high at the end of summer (Fig. 12). Samples collected from CT-VII had a δ^{15}N-NO_3^- range of -4 ‰ to +3 ‰. Samples collected from 15th July 2020 to 11th May 2021 were within the range of -4 ‰ to -2 ‰. Samples collected from CT-II had a δ^{15}N-NO_3^- range of -3 ‰ to +6 ‰. The lowest value, -3.1 ‰, was recorded in the summer and the highest value, 5.2 ‰ recorded in the fall.

4.2.2.2 Čertovo Kendall Plot.

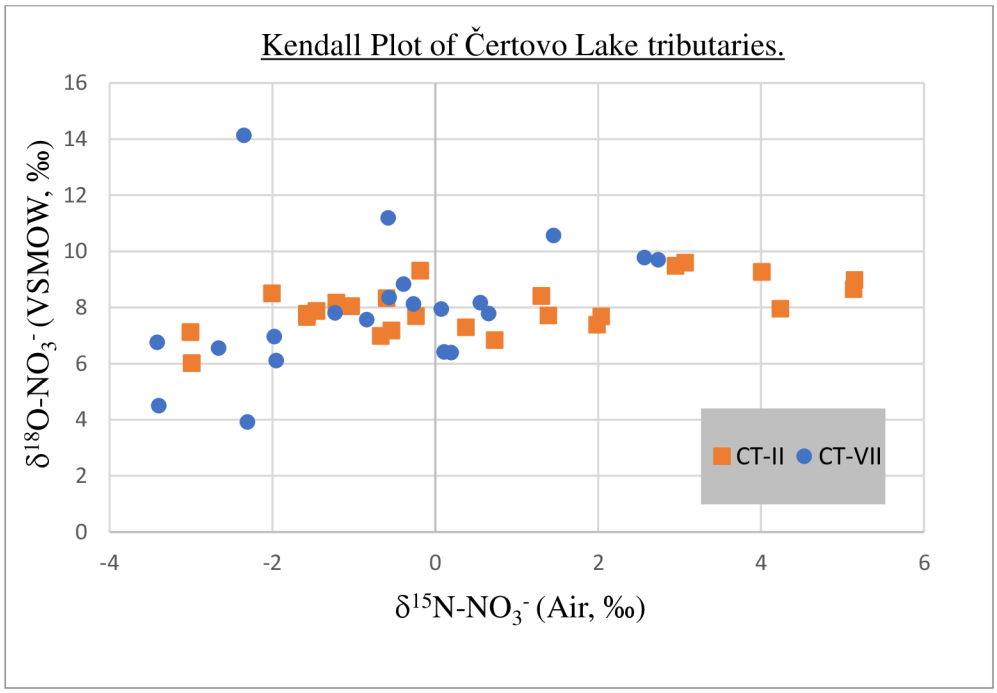

Figure 13: Kendal plot of Čertovo Lake tributaries.

Fig. 13 shows that the samples exhibit a large δ^{15}N-NO_3^- range, from -4 ‰ to +6 ‰. While CT-II did not have a wide range of δ^{18}O-NO_3^- (+6 ‰ to +9.3 ‰), CT-VII had a significantly higher range of δ^{18}O-NO_3^- (+3.9 ‰ to 14. 2 ‰). For CT-II, the data plotted along a significant positive correlation of increasing δ^{15}N- and δ^{18}O-NO_3^- values, with a slope of 0.34 ($R^2 = 0.38$, $p < 0.001$).

4.2.3 Černé

The sample collection site in Černé Lake was the outlet, CN-VY. Samples were collected in summer, winter, and spring. Samples were obtained only from CN-VY because the tributaries were dry for many months. These samples demonstrated a NO_3^--N concentration within the 0.6 to 0.9 ppm range with no apparent trend (data not shown).

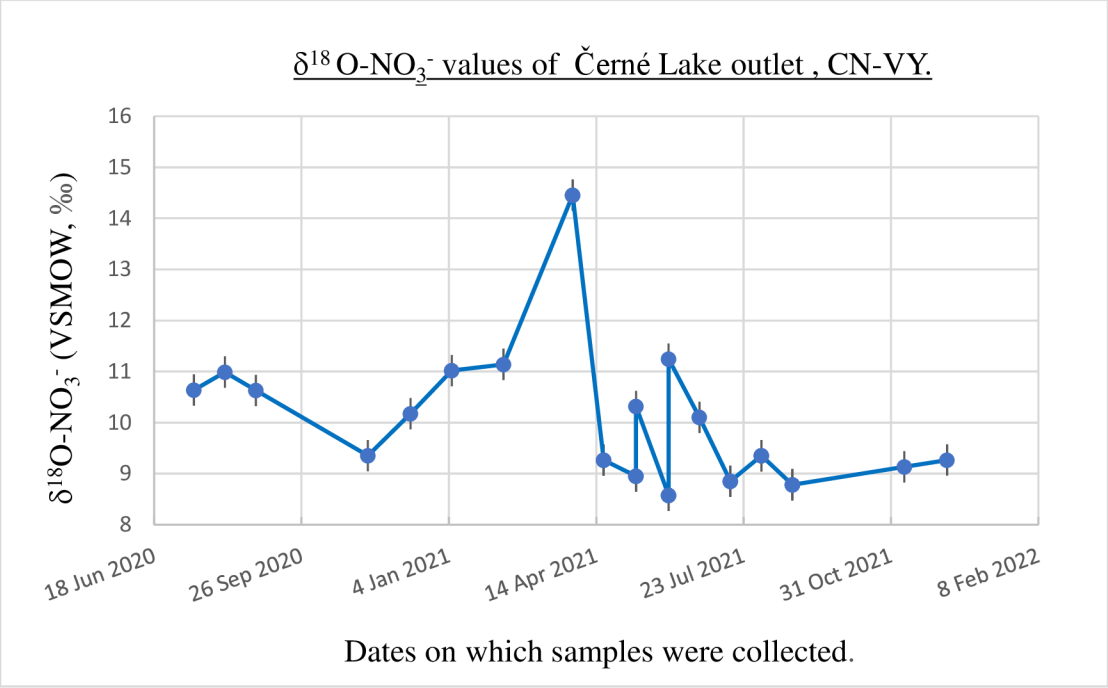

Figure 14. δ ^{18}O-NO_3^- in Černé Lake outlet (CN-VY).

Fig. 14 shows no general pattern in the $\delta^{18}O$-NO_3^- values; one high $\delta^{18}O$-NO_3^- value was measured on 29th March 2021 (+14.5 ‰). In winter (10th November 2020 to 11th February 2021), the values increased from 9.4 ‰ to 11.1 ‰.

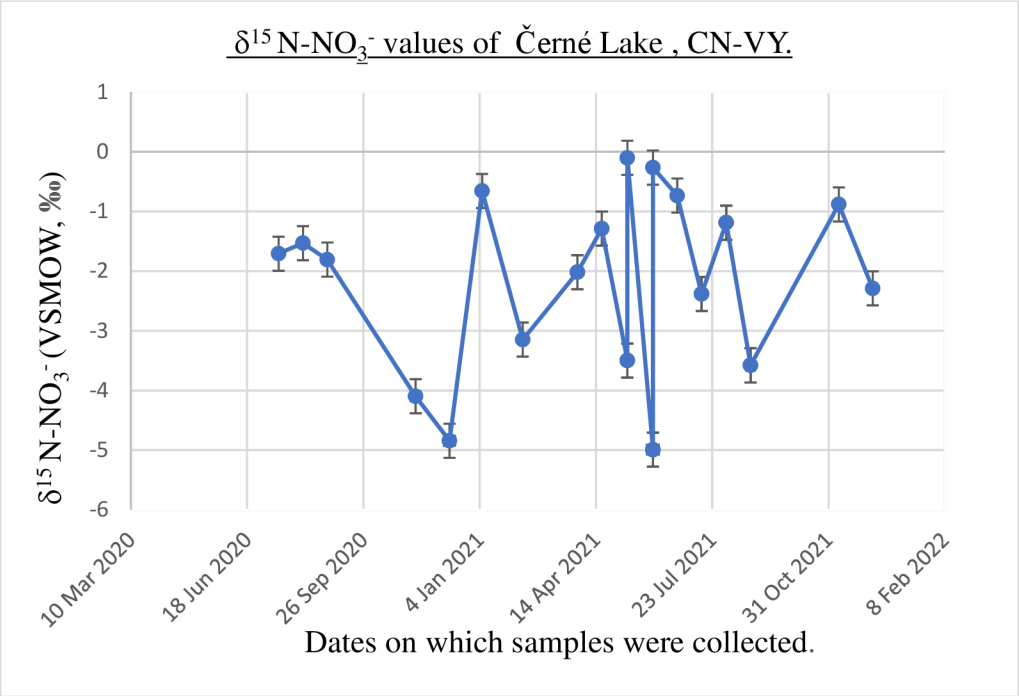

Figure 15: shows the $\delta^{15}N\text{-}NO_3^-$ in Černe Lake outlet, CN-VY.

There was also no systematic pattern in the δ^{15}N-NO3 values. The δ^{15}N values spanned in the negative range, from -5 ‰ to -0.1 ‰.

4.2.3.1 Kendall Plot of Černé Lake.

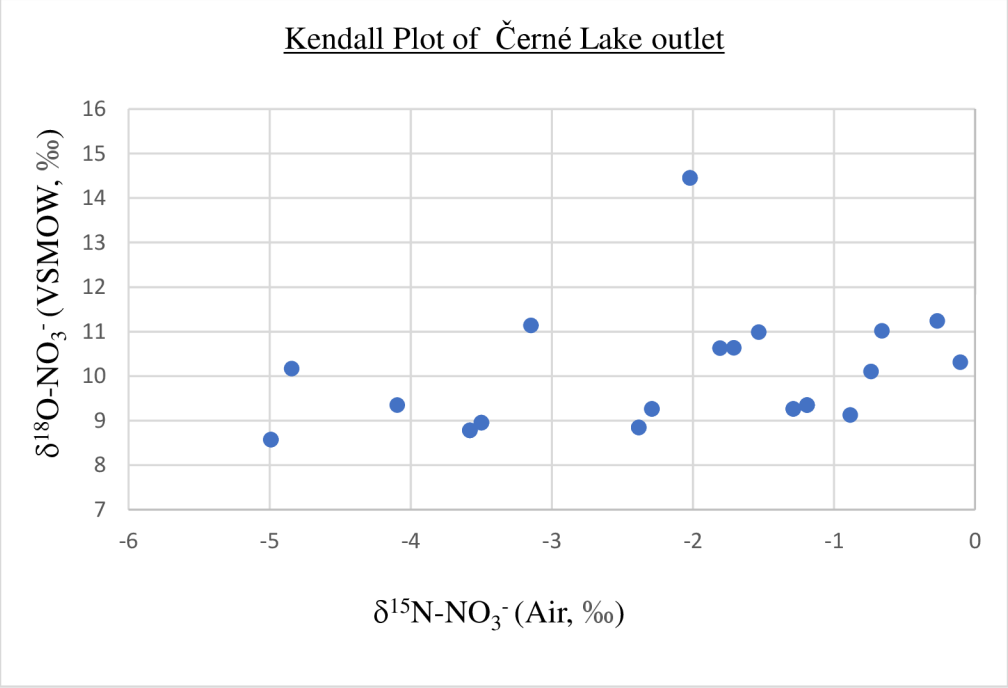

Figure 16: Kendall plot of Černé Lake outlet.

Fig. 16 shows that all observed $\delta^{15}N\text{-}NO_3^-$ values are negative, from -5 ‰ to 0 ‰. The, $\delta^{18}O\text{-}NO_3^-$ values on the other hand, have a positive range between +8 ‰ to 14.5 ‰.

5 Discussion

5.1 Development method to convert nitrate to N2O for stable isotope analysis.

The first goal of the thesis was to compare protocols for converting NO_3^- to N_2O, with attention to preserving the stable isotope composition of NO_3^- in the N_2O molecule. The critical parameters for assessing the performance of the conversion method were the peak amplitude (Ampl 44) and area (Area All, comprising the peaks for masses 44, 45, and 46), and the precision of the isotope measurements (δ values). The first two are related to the yield of the reaction, with higher yield giving higher Ampl 44 and Area All. The exact δ values of the in-house standards were irrelevant for testing the method's performance but are considered later only for normalizing to international reference scales. Analysis of "process blanks" for all methods indicated no significant N_2O peaks (data not shown), therefore, higher "Ampl 44" in the adapted IAEA method was not likely due to trace N_2O (of air) in the headspace. The adapted IAEA method was chosen for future laboratory applications because it gave the best results according to these criteria (Table II). This approach was used for an international inter-laboratory comparison study of nitrate isotopes that was conducted outside the framework of this thesis and achieved the highest "satisfactory" results. Our lab ranked #12 (of 29) globally in performance of determination of $\delta^{18}O\text{-}NO_3^-$ and #22 (of 32) globally in the determination of $\delta^{15}N\text{-}NO_3^-$ (Esquivel-Hernández et al., 2023).

5.2 Comparison of Plešné, Černé and Čertovo lakes, tributaries and outlets using the Kendall Plot.

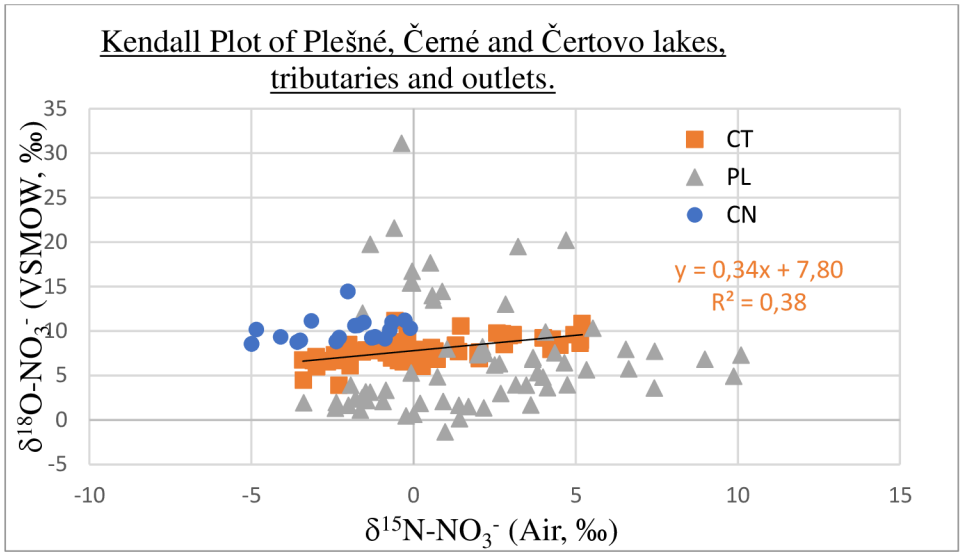

Figure 17: Comparison of NO_3^- isotope values across all the lakes (CT= Čertovo, PL= Plešné, CN = Černé). The solid line and orange text represent the linear regression of CT-II samples. Precipitation samples are omitted from the plot.

A comparison of NO_3^- δ values across the lakes (Fig. 17) reveals that Plešné typically exhibited the lowest $\delta^{18}O\text{-}NO_3^-$ values and Černé the highest $\delta^{18}O\text{-}NO_3^-$ values (excluding some PL samples with high contributions of atmospheric N). These differences likely occur due to distinct, intrinsic N cycling processes in the various catchments, representing the unique balance of input, assimilation, mineralization, nitrification, and denitrification processes. Černé Lake stands out in Fig. 17 due to its higher $\delta^{18}O\text{-}NO_3^-$ levels relative to Plešné and Čertovo Lakes and its exclusively negative $\delta^{15}N\text{-}NO_3^-$ values. This pattern suggests that the NO_3^- source in Černé Lake is more strongly influenced by atmospheric N deposition. As Moore (1977) and Heaton (1990) point out, N from anthropogenic sources, such as automobile emissions (with a $\delta^{15}N\text{-}NO_3^-$ value of 3.7 ‰) and coal-fired plant emissions (ranging from +6 ‰ to +13 ‰), often has greater $\delta^{15}N\text{-}NO_3^-$ values. Kendall et al. (2007) reported that $\delta^{15}N$ of atmospheric NO_3^- may range from -15 ‰ to +15 ‰, with lower values most likely derived from natural NO_X sources such as biogenic soil emissions and lightning. The negative $\delta^{15}N\text{-}NO_3^-$ values observed in the Černé Lake catchment may also be attributed to a potentially higher nitrogen fixation (cf. Fogel and Cifuentes, 1993). As discovered in their research, bacteria that use the enzyme nitrogenase frequently create organic molecules with ^{15}N values slightly below 0 ‰ from atmospheric nitrogen, ranging from -3 ‰ to +1 ‰. Compared to other processes, lower ^{15}N values in organic matter are typically suggestive of N fixation.

5.3 Individual Lakes Discussion.

5.3.1. Plešné

The higher NO_3^--N levels reported in PL during winter may be related to the nitrification processes occurring in the lake (and its tributaries) during this season, when ice may cover the lake. Because light inhibits nitrification (Merbt et al., 2011), the lower light conditions in winter favour increased nitrifier activity. These data are also consistent with earlier observations of increased [NO_3^-] in Wisconsin lakes during winter, which was positively correlated with the duration of ice cover and attributed to benthic mineralization processes (Powers et al., 2017; Powers, Labou et al., 2017). Presumably, in Plešné, benthic mineralization (i.e., nitrification) in winter could outpace N assimilation by phytoplankton and lead to NO_3^- accumulation in the lake.

In PL-HL, [NO_3^--N] ranged between 0.07 ppm to 0.311 ppm in 2021, which is lower than the average concentration documented by Vrba et al. (1996) from 1990-1994, which was 370 µg/L (0.375 ppm). This decline in NO_3^- concentration is attributed to the reduced atmospheric deposition of NO_3^- (Kopáček et al., 2011,2013), indicating a decrease in atmospheric pollution (Kopáček et al., 2013). In mid-spring, there was a significant increase in δ^{18}O-NO_3^- values from samples from the lake outlet. This observed increase may be because of snowmelt carrying nitrate with higher δ^{18}O-NO_3^- values (Williams & Mélack, 1989; Herath et al., 2022).

5.3.2. Čertovo

The seasonal δ^{15}N-NO_3^- signal in CT was marked by high δ^{15}N-NO_3^- values at the end of summer, and that may be associated with apparent denitrification when the lake is also stratified, and other soil conditions may lead to anoxia in the CT catchment. This finding is consistent with that of Kopáček et al. (2006), who reported that denitrification was the largest source of N loss in the CT catchment from 2001-2005. The entire dataset of δ^{15}N-NO_3^- and δ^{18}O-NO_3^- values from 2021-2022 for tributary samples collected from CT plot along an apparent trajectory that is consistent with denitrification, such that δ^{15}N-NO_3^- increases twice as much as δ^{18}O-NO_3^- (slope = 0.35, $p < 0.001$; Fig. 17). This further supports the conclusion that denitrification dominates the N cycling processes in this catchment, particularly for N in the soil that is leached to the lake tributaries.

5.3.3 Černé

For Černé Lake, the $\delta^{18}O\text{-}NO_3^-$ values varied by < 3 ‰ seasonally, with a significant increase in $\delta^{18}O\text{-}NO_3^-$ in March 2021, likely resulting from the snow melt that year. This signal was not observed in $\delta^{15}N\text{-}NO_3^-$, which is consistent with atmospheric NO_3^- deposited with the snow having a higher $\delta^{18}O\text{-}NO_3^-$ value (Fig. 2). Further investigation is required to assess why NO_3^- in this lake consistently exhibited $\delta^{15}N$ values < 0 ‰. This could be a result of relatively higher inputs from N-fixation. This assumption is consistent with Delwiche et al. (1979) findings that in the Kuroshio, surface particulate and dissolved inorganic N pools often had a ^{15}N-depleted isotopic signature, which was attributed to N-fixation. The relatively low $\delta^{15}N\text{-}NO_3^-$ values may also be explained by the relative absence of denitrification in this setting.

6 Conclusion

A titanium reduction method for determining the stable isotope composition of nitrate was developed and tested and was found to achieve satisfactory precision (< 1 per mille) and to be applicable to samples with > 0.2 ppm NO_3^--N. A comparison of nitrate isotope composition in lake samples revealed signals that may arise from various natural processes, including atmospheric deposition, ice cover, summer denitrification, nitrogen fixation and nitrification. For Plešné, high $\delta^{18}O\text{-}NO_3^-$ values in the lake and outlet were attributed to atmospheric nitrogen that appeared to flow through the catchment without being processed by vegetation. For Čertovo, high $\delta^{15}N\text{-}NO_3^-$ values in the lake tributaries at the end of summer depicted denitrification as the major ongoing process determining nitrate isotope composition in the lake catchment. Although further investigation is required to assess why $\delta^{15}N\text{-}NO_3^-$ values in Černé were always < 0 ‰, it can be assumed that the major process ongoing in this lake is nitrogen fixation and/or denitrification had a relatively minor impact on N cycling. The natural processes controlling nitrate isotope values in these lakes may be used to contrast other systems subject to anthropogenic activities, which may exhibit excursions in δ values that cannot be explained by the natural processes identified here. This study could thus be applied to improve risk assessment and efficient management practices in affected systems. Future scientific research could centre around mechanisms that differentiate nitrogen isotope signatures amongst the lakes.

References

Alimi, H., Ertel, T., & Schug, B. (2003). Fingerprinting of Hydrocarbon fuel Contaminants: Literature review. *Environmental Forensics*, *4*(1), 25–38. https://doi.org/10.1080/15275920303489

Altabet, M. A., Wassenaar, L. I., Douence, C., & Roy, R. (2019). A Ti(III) reduction method for one-step conversion of seawater and freshwater nitrate into N2O for stable isotopic analysis of 15N/14N, 18O/16O and 17O/16O. *Rapid Communications in Mass Spectrometry*, *33*(15), 1227–1239. https://doi.org/10.1002/rcm.8454

Ambus, P., & Zechmeister-Boltenstern, S. (2007). Denitrification and N-Cycling in forest ecosystems. In *Elsevier eBooks* (pp. 343–358). https://doi.org/10.1016/b978-044452857-5.50023-0

Appl, M. (2006). Ammonia. *Ullmann's Encyclopedia of Industrial Chemistry*. https://doi.org/10.1002/14356007.a02_143.pub2

Baker, M. A., Dahm, C. N., & Valett, H. M. (2000). Anoxia, anaerobic metabolism, and biogeochemistry of the Stream-water–Ground-water interface. In *Elsevier eBooks* (pp. 259–283). https://doi.org/10.1016/b978-012389845-6/50012-0

Clark, I. D., & Fritz, P. (2013). Environmental isotopes in hydrogeology. In *CRC Press eBooks*. https://doi.org/10.1201/9781482242911

Dawson, T. E., & Brooks, P. D. (2001). Fundamentals of stable isotope Chemistry and Measurement. In *Current plant science and biotechnology in agriculture* (pp. 1–18). https://doi.org/10.1007/978-94-015-9841-5_1

Delwiche, C. C., Zinke, P. J., Johnson, C. M., & Virginia, R. A. (1979). Nitrogen isotope distribution as a presumptive indicator of nitrogen fixation. *Botanical Gazette*, *140*, S65–S69. https://doi.org/10.1086/337037

Esquivel-Hernández, G., Matiatos, I., Sánchez-Murillo, R., Vystavna, Y., Balestrini, R., Hipsey, M., Monteiro, L. R., Chantara, S., Walters, W. W., & Wassenaar, L. I. (2023). Nitrate isotopes (δ 15 N, δ 18 O) in precipitation: best practices from an international coordinated research project. *Isotopes in Environmental and Health Studies*, *59*(2), 127–141. https://doi.org/10.1080/10256016.2023.2177649

Fogel, M. L., & Cifuentes, L. A. (1993). Isotope Fractionation during Primary Production. In *Topics in geobiology* (pp. 73–98). https://doi.org/10.1007/978-1-4615-2890-6_3

Galloway, J. N., Townsend, A. R., Erisman, J. W., Bekunda, M., Cai, Z., Freney, J. R., Martinelli, L. A., Seitzinger, S. P., & Sutton, M. A. (2008). Transformation of the nitrogen Cycle: recent trends, questions, and potential solutions. *Science*, *320*(5878), 889–892. https://doi.org/10.1126/science.1136674

Heaton, T. (1990). 15N/14N ratios of NOx from vehicle engines and coal-fired power stations. *Tellus B*, *42*(3), 304–307. https://doi.org/10.1034/j.1600-0889.1990.00007.x-i1

Herath, I. K., Wu, S., Ma, M., & Huang, P. (2022). Reservoir NO3− pollution and chemical weathering: by dual isotopes of δ15N-NO3−, δ18O-NO3− and geochemical constraints. *Environmental Geochemistry and Health*, *44*(12), 4381–4402. https://doi.org/10.1007/s10653-021-01195-4

Hochman, G., Goldman, A. S., & Felder, F. A. (2022). Alternative ammonia production processes and the use of renewables. In *Elsevier eBooks* (pp. 243–258). https://doi.org/10.1016/b978-0-12-819242-9.00007-5

Kaushal, S. S., Groffman, P. M., Band, L. E., Elliott, E. M., Shields, C. A., & Kendall, C. (2011). Tracking nonpoint source nitrogen pollution in Human-Impacted watersheds. *Environmental Science & Technology*, *45*(19), 8225–8232. https://doi.org/10.1021/es200779e

Kendall, C., Elliot, E. M., & Wankel, S. D. (2007). Tracing anthropogenic inputs of nitrogen to ecosystems. In R. H. Michener & K. Lajtha (Eds.), *Stable isotopes in ecology and environmental science* (2nd ed.). 375–435. https://doi.org/10.1002/9780470691854

Kopáček, J., Fluksová, H., Kaňa, J., Porcal, P., Turek, J., & Žaloudík, J. (2013). Chemical composition of atmospheric deposition in the catchments of Plešné and Čertovo lakes in 1998–2012. *Silva Gabreta*, *19*, 1–23.

Kopáček, J., Turek, J., Hejzlar, J., Kaňa, J., & Porcal, P. (2006). Element fluxes in watershed-lake ecosystems recovering from acidification: Plešné Lake, the Bohemian Forest, 2001–2005. *Biologia*, *61*(S20), S427–S440. https://doi.org/10.2478/s11756-007-0067-7

Kopáček, J., Turek, J., Hejzlar, J., & Porcal, P. (2011). Bulk deposition and throughfall fluxes of elements in the Bohemian Forest (central Europe) from 1998 to 2009. *Boreal Environment Research*, *16*, 495–508. https://helda.helsinki.fi/server/api/core/bitstreams/7b99faa6-ed68-4241-92e7-bac4234e9d8e/content

Kowalchuk, G. A., & Stephen, J. (2001). Ammonia-Oxidizing Bacteria: A model for Molecular Microbial Ecology. *Annual Review of Microbiology*, *55*(1), 485–529. https://doi.org/10.1146/annurev.micro.55.1.485

Kremser, U., & Schnug, E. (2002). Impact of fertilizers on aquatic ecosystems and protection of water bodies from mineral nutrients. *ResearchGate*. https://www.researchgate.net/publication/240641590

Kuveke, R. E. H., Barwise, L., Van Ingen, Y., Vashisth, K., Nj, R., Chitnis, S. S., Dutton, J. L., Martin, C. D., & Melen, R. L. (2022). An international study evaluating elemental analysis. *ACS Central Science*, *8*(7), 855–863. https://doi.org/10.1021/acscentsci.2c00325

Kuypers, M. M. M., Lavik, G., Woebken, D., Schmid, M., Fuchs, B. M., Amann, R., Jørgensen, B. B., & Jetten, M. S. M. (2005). Massive nitrogen loss from the Benguela upwelling

system through anaerobic ammonium oxidation. *Proceedings of the National Academy of Sciences of the United States of America*, *102*(18), 6478–6483. https://doi.org/10.1073/pnas.0502088102

Li, J., Brejcha, J., & Michalski, G. (2019). *Optimizing the N and O isotopic analysis technique of nitrate using Ti(III) reduction method*. NASA/ADS. Retrieved 15th November, 2023, from https://ui.adsabs.harvard.edu/abs/2019AGUFM.U14C..16L/abstract

Liu, M., Mande, S. A., Tchakala, I., Djanéyé-Boundjou, G., & Chen, H. (2014). Tracking sources of groundwater nitrate contamination using nitrogen and oxygen stable isotopes at Beijing area, China. *Environmental Earth Sciences*, *72*(3), 707–715. https://doi.org/10.1007/s12665-013-2994-7

Lukavský, J. (2009). Algae, Cyanobacteria and Chytridiales of Černé Lake in the Bohemian Forest (Šumava, Czech Republic). *Silva Gabreta*, *15*, 2–3. https://www.npsumava.cz/wp-content/uploads/2019/06/sg_15_1_lukavsky.pdf

Marchant, H. K., Ahmerkamp, S., Lavik, G., Tegetmeyer, H. E., Graf, J. S., Klatt, J. M., Holtappels, M., Walpersdorf, E., & Kuypers, M. M. M. (2017). Denitrifying community in coastal sediments performs aerobic and anaerobic respiration simultaneously. *The ISME Journal*, *11*(8), 1799–1812. https://doi.org/10.1038/ismej.2017.51

McIlvin, M. R., & Altabet, M. A. (2005). Chemical conversion of nitrate and nitrite to nitrous oxide for nitrogen and oxygen isotopic analysis in freshwater and seawater. *Analytical Chemistry*, *77*(17), 5589–5595. https://doi.org/10.1021/ac050528s

Merbt, S. N., Stahl, D. A., Casamayor, E. O., Martı, E., Nicol, G. W., & Prosser, J. I. (2011). Differential photoinhibition of bacterial and archaeal ammonia oxidation. *FEMS Microbiology Letters*, *327*(1), 41–46. https://doi.org/10.1111/j.1574-6968.2011.02457.x

Michener, R. H., & Lajtha, K. (2007). Stable isotopes in ecology and environmental science. In *Wiley eBooks*. https://doi.org/10.1002/9780470691854

Moore, H. E. (1977). The isotopic composition of ammonia, nitrogen dioxide and nitrate in the atmosphere. *Atmospheric Environment*, *11*(12), 1239–1243. https://doi.org/10.1016/0004-6981(77)90102-0

Morot-Gaudry, J. (2001). Nitrogen assimilation by plants. In *CRC Press eBooks*. https://doi.org/10.1201/9781482279849

Munch, J. C., & Velthof, G. (2007). Denitrification and agriculture. In *Elsevier eBooks* (pp. 331–341). https://doi.org/10.1016/b978-044452857-5.50022-9

Nestler, A., Berglund, M., Accoe, F., Duta, S., Xue, D., Boeckx, P., & Philip, T. (2011). Isotopes for improved management of nitrate pollution in aqueous resources: review of surface water field studies. *Environmental Science and Pollution Research*, *18*(4), 519–533. https://doi.org/10.1007/s11356-010-0422-z

O, M. J., Ruth, W., Jane, M., & Charles, O. (2013). A research paper on the analysis of the levels of nitrate in homemade brews spirits in water and raw materials in Nairobi County. *International Journal of Scientific & Technology Research*, *2*(6), 14–19. https://www.ijstr.org/final-print/june2013/A-Research-Paper-On-The-Analysis-Of-The-Levels-Of-Nitrate-In-Homemade-Brews-Spirits-In-Water-And-Raw-Materials-In-Nairobi-County.pdf

Ostrom, N. E., & Ostrom, P. H. (2006). Nitrogen isotopesisotopes. In *Kluwer Academic Publishers eBooks* (pp. 431–434). https://doi.org/10.1007/1-4020-4496-8_215

Porcal, P., Kopáček, J., & Tomková, I. (2014). Seasonal photochemical transformations of nitrogen species in a forest stream and lake. *PLOS ONE*, *9*(12), e116364. https://doi.org/10.1371/journal.pone.0116364

Powers, S. M., Baulch, H. M., Hampton, S. E., Labou, S., Lottig, N. R., & Stanley, E. H. (2017). Nitrification contributes to winter oxygen depletion in seasonally frozen forested lakes. *Biogeochemistry*, *136*(2), 119–129. https://doi.org/10.1007/s10533-017-0382-1

Powers, S. M., Labou, S., Baulch, H. M., Hunt, R. J., Lottig, N. R., Hampton, S. E., & Stanley, E. H. (2017). Ice duration drives winter nitrate accumulation in north temperate lakes. *Limnology and Oceanography Letters*, *2*(5), 177–186. https://doi.org/10.1002/lol2.10048

Qu, Z., Bakken, L. R., Molstad, L., Frostegård, Å., & Bergaust, L. (2016). Transcriptional and metabolic regulation of denitrification in Paracoccus denitrificans allows low but significant activity of nitrous oxide reductase under oxic conditions. *Environmental Microbiology*, *18*(9), 2951–2963. https://doi.org/10.1111/1462-2920.13128

Risgaard-Petersen, N., Langezaal, A., Ingvardsen, S., Schmid, M., Jetten, M. S. M., Camp, H. J. M. O. D., Derksen, J., Piña-Ochoa, E., Eriksson, S. P., Nielsen, L. P., Revsbech, N. P., Cedhagen, T., & Van Der Zwaan, G. (2006). Evidence for complete denitrification in a benthic foraminifer. *Nature*, *443*(7107), 93–96. https://doi.org/10.1038/nature05070

Seitzinger, S. P. (1988). Denitrification in freshwater and coastal marine ecosystems: Ecological and geochemical significance. *Limnology and Oceanography*, *33*(4part2), 702–724. https://doi.org/10.4319/lo.1988.33.4part2.0702

Sigman, D. M., Casciotti, K. L., Andréani, M., Barford, C., Galanter, M., & Böhlke, J. K. (2001). A bacterial method for the nitrogen isotopic analysis of nitrate in seawater and freshwater. *Analytical Chemistry*, *73*(17), 4145–4153. https://doi.org/10.1021/ac010088e

Smil, V. (1999). Detonator of the population explosion. *Nature*, *400*(6743), 415. https://doi.org/10.1038/22672

Stein, L. Y., & Klotz, M. G. (2016). The nitrogen cycle. *Current Biology*, *26*(3), R94–R98. https://doi.org/10.1016/j.cub.2015.12.021

Strous, M., Fuerst, J. A., Kramer, E. H. M., Logemann, S., Muyzer, G., Van De Pas-Schoonen, K. T., Webb, R. I., Kuenen, J., & Jetten, M. S. M. (1999). Missing lithotroph identified as new planctomycete. *Nature*, *400*(6743), 446–449. https://doi.org/10.1038/22749

Sulzman, E. W. (2007). Stable Isotope Chemistry and Measurement: a primer. In R. H. Michener & K. Lajtha (Eds.), *Stable isotopes in ecology and environmental science* (2nd ed.). 1–18. https://doi.org/10.1002/9780470691854

Takai, K. (2019). The nitrogen cycle: a large, fast, and mystifying cycle. *Microbes and Environments*, *34*(3), 223–225. https://doi.org/10.1264/jsme2.me3403rh

Vrba, J., Kopáček, J., Straškrabová, V., Hejzlar, J., & Šimek, K. (1996). Limnological research of acidified lakes in Czech part of the Šumava mountains:trophic status and dominance of microbial food webs. *Silva Gabreta*, *1*, 151–164. https://www.npsumava.cz/wp-content/uploads/2019/06/sg1_vrbaetal.pdf

Ward, B. (1996). Nitrification and ammonification in aquatic systems. *PubMed*, *3*(1–2), 25–29. https://pubmed.ncbi.nlm.nih.gov/11539155

Williams, M. W., & Mélack, J. M. (1989). Effects of spatial and temporal variation in snow melt on nitrate ion and sulfate ion pulses in melt waters within an alpine basin. *Annals of Glaciology*, *13*, 285–288. https://doi.org/10.1017/s0260305500008065

Wright, L. E. (2016). Oxygen isotopes. In *Encyclopedia of earth sciences* (pp. 567–574). https://doi.org/10.1007/978-1-4020-4409-0_22

Xu, S., Kang, P., & Sun, Y. (2015). A stable isotope approach and its application for identifying nitrate source and transformation process in water. *Environmental Science and Pollution Research*, *23*(2), 1133–1148. https://doi.org/10.1007/s11356-015-5309-6

Appendix

Appendix 1: Sequence template for 200 ppb NO_3^- -N analysis.

		NO_3-N	Sample	NO_3-N	DI water	$TiCl_3$	Total Vol.
	Sample	mg L^{-1}	uL	mg	uL	uL	uL
1	MiiliQ blank	0.00	0	0.0000	3000	100	3100
2	USGS34	1.00	600	0.0006	2400	100	3100
3	USGS34	1.00	600	0.0006	2400	100	3100
4	USGS35	1.00	600	0.0006	2400	100	3100
5	MIX 32/34	1.00	300+300	0.0006	2400	100	3100
6	USGS32	1.00	600	0.0006	2400	100	3100
7	KNO_3_IHS	1.00	600	0.0006	2400	100	3100
8	KNO_3_IHS_TSR3	1.00	900	0.0009	2100	100	3100
9	KNO_3_IHS_TSR2	1.00	400	0.0004	2600	100	3100
10	KNO_3_IHS_TSR1	1.00	300	0.0003	2700	100	3100
11	sample1	3.23	190	0.0006	2810	100	3100
12	sample2	2.36	250	0.0006	2750	100	3100
13	sample3	2.51	240	0.0006	2760	100	3100
14	sample4	2.92	210	0.0006	2790	100	3100
15	sample5	0.60	1000	0.0006	2000	100	3100
16	sample6	0.29	2070	0.0006	930	100	3100
17	sample7	0.47	1280	0.0006	1720	100	3100
18	sample8	0.34	1760	0.0006	1240	100	3100
19	sample9	0.34	1760	0.0006	1240	100	3100
20	sample10	0.18	3000	0.0005	0	100	3100
21	sample11	0.40	1500	0.0006	1500	100	3100
22	sample12	0.20	3000	0.0006	0	100	3100
23	sample13	0.18	3000	0.0005	0	100	3100
24	sample14	0.40	1500	0.0006	1500	100	3100
25	sample15	0.20	3000	0.0006	0	100	3100
26	MiiliQ blank	0.00	0	0.0000	3000	100	3100
27	USGS34	1.00	600	0.0006	2400	100	3100
28	USGS34	1.00	600	0.0006	2400	100	3100
29	USGS35	1.00	600	0.0006	2400	100	3100

30	USGS32	1.00	600	0.0006	2400	100	3100
31	MIX 32/34	1.00	300+300	0.0006	2400	100	3100
32	KNO_3_IHS	1.00	600	0.0006	2400	100	3100
33	sample16	0.17	3000	0.0005	0	100	3100
34	sample17	0.32	1880	0.0006	1120	100	3100
35	sample18	0.27	2220	0.0006	780	100	3100
36	sample19	0.12	3000	0.0004	0	100	3100
37	sample20	0.21	2860	0.0006	140	100	3100
38	sample21	0.07	3000	0.0002	0	100	3100
39	sample22	0.12	3000	0.0004	0	100	3100
40	sample23	0.11	3000	0.0003	0	100	3100
41	sample24	0.15	3000	0.0005	0	100	3100
42	sample25	0.21	2860	0.0006	140	100	3100
43	sample26	0.19	3000	0.0006	0	100	3100
44	sample27	0.14	3000	0.0004	0	100	3100
45	sample28	0.18	3000	0.0005	0	100	3100
46	sample29	0.40	1500	0.0006	1500	100	3100
47	sample30	0.20	3000	0.0006	0	100	3100
48	MiiliQ blank	0.00	0	0.0000	3000	100	3100
49	USGS34	1.00	600	0.0006	2400	100	3100
50	USGS35	1.00	600	0.0006	2400	100	3100
51	USGS35	1.00	600	0.0006	2400	100	3100
52	USGS32	1.00	600	0.0006	2400	100	3100
53	MIX 32/34	1.00	300+300	0.0006	2400	100	3100
54	KNO_3_IHS	1.00	600	0.0006	2400	100	3100
55	sample31	0.17	3000	0.0005	0	100	3100
56	sample32	0.32	1880	0.0006	1120	100	3100
57	sample33	0.27	2220	0.0006	780	100	3100
58	sample34	0.12	3000	0.0004	0	100	3100
59	sample35	0.21	2860	0.0006	140	100	3100
60	sample36	0.07	3000	0.0002	0	100	3100
61	sample37	0.12	3000	0.0004	0	100	3100
62	sample38	0.11	3000	0.0003	0	100	3100
63	sample39	0.15	3000	0.0005	0	100	3100

64	sample40	0.21	2860	0.0006	140	100	3100
65	sample41	0.19	3000	0.0006	0	100	3100
66	sample42	0.14	3000	0.0004	0	100	3100
67	sample43	0.21	2860	0.0006	140	100	3100
68	sample44	0.19	3000	0.0006	0	100	3100
69	sample45	0.14	3000	0.0004	0	100	3100
70	MiiliQ blank	0.00	0	0.0000	3000	100	3100
71	USGS34	1.00	600	0.0006	2400	100	3100
72	USGS35	1.00	600	0.0006	2400	100	3100
73	USGS32	1.00	600	0.0006	2400	100	3100
74	USGS32	1.00	600	0.0006	2400	100	3100
75	MIX 32/34	1.00	300+300	0.0006	2400	100	3100
76	MIX 32/34	1.00	300+300	0.0006	2400	100	3100
77	Air blank	0.00	0	0.0000	3000	100	3100